Characteristics of Beam-based Flexure Modules

Submitted to the ASME Journal of Mechanical Design

Authors

Shorya Awtar[1]
Precision Engineering Research Group
Massachusetts Institute of Technology, Cambridge MA
518-577-5500, shorya@mit.edu

Alexander H. Slocum
Precision Engineering Research Group
Massachusetts Institute of Technology, Cambridge MA
617-253-0012, slocum@mit.edu

Edip Sevincer
Omega Advanced Solutions Inc., Troy NY
518-276-8191, sevincer@omegaadvanced.com

Abstract

The beam flexure is an important constraint element in flexure mechanism design. Non-linearities arising from the force equilibrium conditions in a beam significantly affect its properties as a constraint element. Consequently, beam-based flexure mechanisms suffer from performance tradeoffs in terms of motion range, accuracy and stiffness, while benefiting from elastic averaging. This paper presents simple yet accurate approximations that capture the effects of load-stiffening and elastokinematic non-linearities in beams. A general analytical framework is developed that enables a designer to parametrically predict the performance characteristics such as mobility, over-constraint, stiffness variation, and error motions, of beam-based flexure mechanisms without resorting to tedious numerical or computational methods. To illustrate their effectiveness, these approximations and analysis approach are used in deriving the force-displacement relationships of several important beam-based flexure constraint modules, and the results are validated using Finite Element Analysis. Effects of variations in shape and geometry are also analytically quantified.

[1] Corresponding Author

Keywords: Beam Flexure, Parallelogram Flexure, Tilted-beam Flexure, Double Parallelogram Flexure, Double Tilted-beam Flexure, Non-linear Beam Analysis, Elastokinematic Effect, Flexure Design Tradeoffs

1. Introduction and Background

From the perspective of precision machine design [1-4], flexures are essentially constraint elements that utilize material elasticity to allow small yet frictionless motions. The objective of an ideal constraint element is to provide infinite stiffness and zero displacements along its *Degrees of Constraint* (DOC), and allow infinite motion and zero stiffness along its *Degrees of Freedom* (DOF). Clearly, flexures deviate from ideal constraints in several ways, the primary of which is limited motion along the DOF. Given a maximum allowable stress, this range of motion can be improved by choosing a distributed-compliance topology over its lumped-compliance counterpart, as illustrated in Fig. 1. However, distribution of compliance in a flexure mechanism gives rise to non-linear elastokinematic effects, which result in two very important attributes. Firstly, the error motions and stiffness values along the DOC deteriorate with increasing range of motion along DOF, which leads to fundamental performance tradeoffs in flexures [5]. Secondly, distributed compliance enables elastic averaging and allows non-exact constraint designs that are otherwise unrealizable. For example, while the lumped-compliance multi-parallelogram flexure in Fig. 1a is prone to over-constraint in the presence of typical manufacturing and assembly errors, its distributed-compliance version of Fig. 1b is relatively more tolerant. Elastic averaging greatly opens up the design space for flexure mechanisms by allowing special geometries and symmetric layouts that offer performance benefits [5]. Thus, distributed compliance in flexure mechanisms results in desirable as well as undesirable attributes, which coexist due to a common root cause. Because of their influence on constraint behavior, it is important to understand and characterize these attributes while pursuing systematic constraint-based flexure mechanism design.

The uniform-thickness beam flexure is a classic example of a distributed-compliance topology. With increasing displacements, non-linearities in force-displacement relationships of a beam flexure can arise from one of three sources – material constitutive properties, geometric compatibility, and force equilibrium conditions. While the beam material is typically linear-

elastic, the geometric compatibility condition between the beam's curvature and displacement is an important source of non-linearity. In general, this non-linearity becomes significant for transverse displacements of the order of one-tenth the beam length, and has been thoroughly analyzed in the literature using analytical and numerical methods [6-8]. Simple and accurate parametric approximations based on the pseudo-rigid body method also capture this non-linearity and have proven to be important tools in the design and analysis of mechanisms with large displacements [9]. However, the non-linearity resulting from the force equilibrium conditions can become significant for transverse displacements as small as the beam thickness. Since this non-linearity captures load-stiffening and elastokinematic effects, it is indispensable in determining the influence of loads and displacements on the beam's constraint behavior. These effects truly reveal the design tradeoffs in beam-based flexure mechanisms and influence all the key performance characteristics such as mobility, over-constraint, stiffness variation, and error motions. Although both these non-linear effects have been appropriately modeled in the prior literature, the presented analyses are either unsuited for quick design calculations [10], case-specific [11], or require numerical/graphical solution methods [12-13]. While pseudo-rigid body models capture load-stiffening, their inherent lumped-compliance assumption precludes elastokinematic effects.

Since we are interested in transverse displacements that are an order of magnitude less than the beam length but generally greater than the beam nominal thickness, this third source of non-linearity is the focus of discussion in this paper. We propose the use of simple polynomial approximations in place of transcendental functions arising from the deformed-state force equilibrium condition in beams. These approximations are shown to yield very accurate closed-form force-displacement relationships of the beam flexure and other beam-based flexure modules, and help quantify the associated performance characteristics and tradeoffs. Furthermore, these closed-form parametric results enable a physical understanding of distributed-compliance flexure mechanism behavior, and thus provide useful qualitative and quantitative design insights.

The term *flexure module* is used in this paper to refer to a flexure building-block that serves as a constraint element in a potentially larger and more complex flexure mechanism. Flexure modules are the simplest examples of flexure mechanisms.

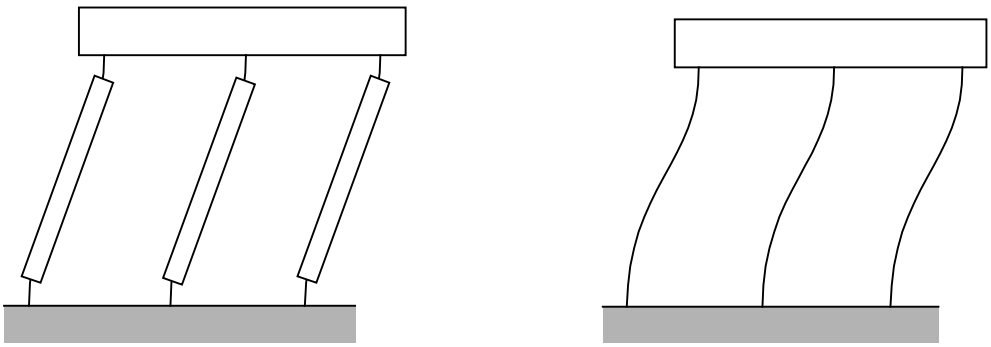

Fig.1 a) Lumped-Compliance and b) Distributed-Compliance Multi-Parallelogram Mechanisms

2. Characteristics of Flexure Modules

This section presents some key performance characteristics that capture the constraint behavior of flexure modules, and will be referred to in the rest of this paper. These include the concepts of mobility (DOF/DOC), stiffness variations, error motions, and Center of Stiffness (COS).

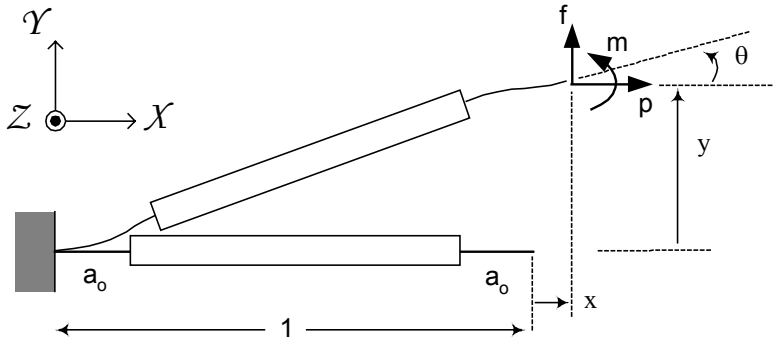

Fig.2 Generalized Beam Flexure

For a flexure module, one may intuitively or analytically assign stiff directions to be Degrees of Constraint and compliant directions to Degrees of Freedom. For example, in the beam flexure illustrated in Fig. 2, the transverse displacements of the beam tip, y and θ, obviously constitute the two Degrees of Freedom, whereas axial direction x displacement is a Degree of Constraint. However, for flexure mechanisms comprising of several distributed-compliance elements, this simplistic interpretation of mobility needs some careful refinement.

In a given module or mechanism, one may identify all possible locations or *nodes*, finite in number, where forces may be allowed. For planer mechanisms, each node is associated with three generalized forces, or *allowable forces*, and three *displacement coordinates*. Under any given set of normalized allowable forces of unit order magnitude, some of these displacement coordinates will assume relatively large values as compared to others. The maximum number of displacement coordinates that can be made *independently* large using any combination of the allowable forces, each of unit order magnitude, quantifies the Degrees of Freedom of the flexure mechanism. The remaining displacement coordinates contribute to the Degrees of Constraint. For obvious reasons, normalized stiffness or compliance not only plays an important role in the determination of DOF and DOC, but also provides a measure for their *quality*. In general, it is always desirable to maximize stiffness along the DOC and compliance along the DOF. Since load-stiffening and elastokinematic effects result in stiffness variations, these non-linearities have to be included for an accurate prediction of the number and quality of DOF and DOC in a distributed-compliance flexure mechanism. A situation where the stiffness along a DOF increases significantly with increasing displacements represents a condition of *over-constraint*. These considerations are not always captured by the traditional Gruebler's criterion.

A second measure of the quality of a DOF or DOC is error motion, which affects the motion accuracy of a given flexure module or mechanism. While it is common to treat any undesired displacement in a flexure mechanism as a parasitic error, we propose a more specific description of error motions. The desired motion, or *primary motion*, is one that occurs in the direction of an applied generalized force along a DOF. Resulting motions in any other direction are deemed as undesired or *error motions*. In a purely linear elastic formulation, this has a straight-forward implication. If the compliance, or alternatively stiffness, matrix relating the allowable forces to the displacement coordinates has any off-diagonal terms, the corresponding forces will generate undesired motions. However, a non-linear formulation reveals load-stiffening, kinematic and elastokinematic effects in the force-displacement relationships, which can lead to additional undesired motions. Since these terms are revealed in a mechanism's deformed configuration, an accurate characterization of undesired motions should be performed by first applying unit order allowable forces in order to nominally deform the mechanism. From this deformed configuration, only the generalized force along the direction of primary motion is varied while others are kept constant. The resulting changes in displacements along all other displacement

coordinates provide a true measure of undesired motions in a mechanism. The undesired motions along the other Degrees of Freedom are defined here as *cross-axis error motion*, while those along the Degrees of Constraint are referred to as *parasitic error motions*. Each of these error motions can be explicitly force dependent, purely kinematic, elastokinematic, or any combination thereof. This shall be illustrated in the following sections by means of specific flexure module examples.

Such a characterization is important because it reveals the constituents of a given error motion. Any error component that is explicitly force dependent, based on either elastic or load-stiffening effects, may be eliminated by an appropriate combination of allowable forces. In some cases, this may be accomplished by simply varying the location of an applied force to provide an additional moment. This observation leads to the concept of *Center of Stiffness (COS)*. If the rotation of a certain stage in a flexure mechanism is undesired, then the particular location of an applied force that results in zero stage rotation is defined as the COS of the mechanism with respect to the given stage and applied force. Obviously, the COS may shift with loading and deformation. Kinematic terms that contribute to error motions are dependent on other displacements and, in general, may not be eliminated by any combination of allowable forces without over-constraining the mechanism. Optimizing the shape of the constituent distributed-compliance elements can only change the magnitude of these kinematic terms while a modification of the mechanism topology is required to entirely eliminate them. Elastokinematic contributions to error motions, on the other hand, can be altered by either of these two schemes – by appropriately selecting the allowable forces, as well as by making geometric changes. This information provides insight regarding the kind of optimization and topological redesign that may be needed to improve the motion accuracy in a flexure mechanism.

3. Beam Flexure

Fig. 2 illustrates a varying-thickness beam with generalized end-forces and end-displacements in a deformed configuration. Displacements and lengths are normalized by the overall beam length L, forces by $E'I_{zz}/L^2$, and moments by $E'I_{zz}/L$. The two equal end-segments have a uniform thickness t, and the middle section is thick enough to be considered rigid. The symbol E' is used

to denote Young's modulus for a state of plane stress, and plate modulus for plane strain. All non-dimensional quantities are represented by lower case letters throughout this discussion.

The case of a simple beam ($a_o=1/2$) is first considered. For transverse displacements, y and θ, of the order of 0.1 or smaller, beam curvature may be linearized by assuming small slopes. Since the force equilibrium condition is applied in the deformed configuration of the beam, the axial force $\boldsymbol{p}$ contributes to the bending moments. Solving Euler's equation for the simple beam yields the following well-known results [3, 10], where the normalized tensile axial force $\boldsymbol{p} \triangleq k^2$.

$$\begin{aligned} \boldsymbol{f} &= \frac{k^3 \sinh k}{k\sinh k - 2\cosh k + 2}\, y + \frac{k^2(1-\cosh k)}{k\sinh k - 2\cosh k + 2}\, \theta \\ \boldsymbol{m} &= \frac{k^2(1-\cosh k)}{k\sinh k - 2\cosh k + 2}\, y + \frac{k^2\cosh k - k\sinh k}{k\sinh k - 2\cosh k + 2}\, \theta \end{aligned} \tag{1}$$

$$\begin{aligned} y &= \left(\frac{k-\tanh k}{k^3}\right)\boldsymbol{f} + \left(\frac{\cosh k - 1}{k^2\cosh k}\right)\boldsymbol{m} \\ \theta &= \left(\frac{\cosh k - 1}{k^2\cosh k}\right)\boldsymbol{f} + \left(\frac{\tanh k}{k}\right)\boldsymbol{m} \end{aligned} \tag{2}$$

$$x = x^e + x^k = \frac{\boldsymbol{p}}{d} - \begin{bmatrix} y & \theta \end{bmatrix}\begin{bmatrix} r_{11} & r_{12} \\ r_{21} & r_{22} \end{bmatrix}\begin{bmatrix} y \\ \theta \end{bmatrix} \tag{3}$$

where, $d = 12/t^2$

$$r_{11} = \frac{k^2(\cosh^2 k + \cosh k - 2) - 3k\sinh k(\cosh k - 1)}{2\left(k\sinh k - 2\cosh k + 2\right)^2}$$

$$r_{12} = r_{21} = -\frac{k^2(\cosh k - 1) + k\ \sinh k\ (\cosh k - 1) - 4(\cosh k - 1)^2}{4\left(k\sinh k - 2\cosh k + 2\right)^2}$$

$$r_{22} = \frac{-k^3 + k^2\sinh k(\cosh k + 2) - 2k\ (2\cosh^2 k - \cosh k - 1)}{4k\left(k\sinh k - 2\cosh k + 2\right)^2} + \frac{2\sinh k\ (\cosh k - 1)}{4k\left(k\sinh k - 2\cosh k + 2\right)^2}$$

In the presence of a compressive axial force, expressions analogous to (1)-(3) may be obtained in terms of trigonometric functions instead of hyperbolic functions. The axial displacement x is comprised of two components – a purely elastic component x^e that results due to the elastic stretching of the beam, and a kinematic component x^k that results from the conservation of beam arc-length. The kinematic component of the axial displacement may be alternatively stated in

terms of the transverse loads $\boldsymbol{f}$ and $\boldsymbol{m}$, instead of displacements y and θ. However, it should be recognized that this component fundamentally arises from a condition of geometric constraint that requires the beam arc-length to stay constant as it takes a new shape.

Based on the approximations made until this stage, the above results should be accurate to within a few percent of the true behavior of an ideal beam. Although the dependence of transverse stiffness on axial force, and axial stiffness on transverse displacement is evident in expressions (1)-(3), their transcendental nature offers little parametric insight to a designer. We therefore propose simplifications that are based on an observation that the transverse compliance terms may be accurately approximated by inverse linear or inverse quadratic expressions.

$$C = \begin{bmatrix} \left(\dfrac{k-\tanh k}{k^3}\right) & \left(\dfrac{\cosh k - 1}{k^2 \cosh k}\right) \\ \left(\dfrac{\cosh k - 1}{k^2 \cosh k}\right) & \left(\dfrac{\tanh k}{k}\right) \end{bmatrix} \approx \begin{bmatrix} \dfrac{1}{3\left(1+\frac{2}{5}\boldsymbol{p}\right)} & \dfrac{1}{2\left(1+\frac{5}{12}\boldsymbol{p}\right)} \\ \dfrac{1}{2\left(1+\frac{5}{12}\boldsymbol{p}\right)} & \dfrac{\left(1+\frac{1}{10}\boldsymbol{p}\right)}{\left(1+\frac{13}{30}\boldsymbol{p}+\frac{1}{96}\boldsymbol{p}^2\right)} \end{bmatrix} \tag{4}$$

A comparison of the series expansions of the actual hyperbolic functions and their respective approximations, provided in the appendix, reveals that the series coefficients remain close even for higher order terms. The actual and approximate functions for the three compliance terms are plotted in Fig. 3 for a range of $\boldsymbol{p} = -2.5$ to 10. Since $\boldsymbol{p} = -\pi^2/4 \approx -2.47$ corresponds to the first fixed-free beam buckling mode $(\boldsymbol{f} = m = 0)$, all the compliance terms exhibit a singularity at this value of $\boldsymbol{p}$. The approximate functions accurately capture this singularity, but only for the first fixed-free beam buckling mode.

The fact that some compliance terms are well approximated by inverse linear functions of the axial force $\boldsymbol{p}$ indicates that the stiffness terms may be approximated simply by linear functions of $\boldsymbol{p}$. These linear approximations are easily obtained from the series expansion of the hyperbolic functions in expression (1), which show that the higher order terms are small enough to be neglected for values of $\boldsymbol{p}$ as large as ± 10.

$$K = \begin{bmatrix} \dfrac{k^3 \sinh k}{k\sinh k - 2\cosh k + 2} & \dfrac{k^2(1-\cosh k)}{k\sinh k - 2\cosh k + 2} \\ \dfrac{k^2(1-\cosh k)}{k\sinh k - 2\cosh k + 2} & \dfrac{k^2\cosh k - k\sinh k}{k\sinh k - 2\cosh k + 2} \end{bmatrix} \approx \begin{bmatrix} 12\left(1+\frac{1}{10}\boldsymbol{p}\right) & -6\left(1+\frac{1}{60}\boldsymbol{p}\right) \\ -6\left(1+\frac{1}{60}\boldsymbol{p}\right) & 4\left(1+\frac{1}{30}\boldsymbol{p}\right) \end{bmatrix} \tag{5}$$

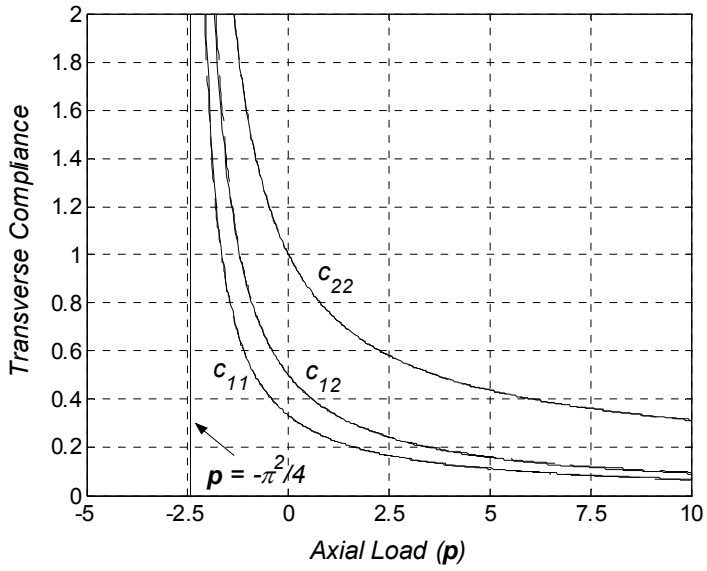

Fig.3 Normalized Compliance Terms: Actual (Solid Lines) and Approximate (Dashed Lines)

Similarly, the following linear approximations can be made for the hyperbolic functions in the geometric constraint relation (3).

$$x^k \approx -\begin{bmatrix} y & \theta \end{bmatrix} \begin{bmatrix} \frac{3}{5}\left(1-\frac{p}{420}\right) & -\frac{1}{20}\left(1-\frac{p}{70}\right) \\ -\frac{1}{20}\left(1-\frac{p}{70}\right) & \frac{1}{15}\left(1-\frac{11p}{420}\right) \end{bmatrix} \begin{bmatrix} y \\ \theta \end{bmatrix} \tag{6}$$

The maximum error in approximation in all of the above cases is less than *3%* for $\boldsymbol{p}$ within ± *10*. This excellent mathematical match between the transcendental functions and their respective approximations has far-reaching consequences in terms of revealing the key characteristics of a beam flexure. Although shown for the tensile axial force case, all of the above approximations hold valid for the compressive case as well. Summarizing the results so far in a general format,

$$\begin{bmatrix} \boldsymbol{f} \\ \boldsymbol{m} \end{bmatrix} = \begin{bmatrix} a & c \\ c & b \end{bmatrix} \begin{bmatrix} y \\ \theta \end{bmatrix} + \boldsymbol{p} \begin{bmatrix} e & h \\ h & g \end{bmatrix} \begin{bmatrix} y \\ \theta \end{bmatrix} \tag{7}$$

$$x = \frac{1}{d}\boldsymbol{p} + \begin{bmatrix} y & \theta \end{bmatrix} \begin{bmatrix} i & k \\ k & j \end{bmatrix} \begin{bmatrix} y \\ \theta \end{bmatrix} + \boldsymbol{p} \begin{bmatrix} y & \theta \end{bmatrix} \begin{bmatrix} r & q \\ q & s \end{bmatrix} \begin{bmatrix} y \\ \theta \end{bmatrix} \tag{8}$$

The coefficients *a*, *b*, *c*, *e*, *g*, *h*, *i*, *j*, *k*, *q*, *r* and *s* are all non-dimensional numbers that are characteristic of the beam shape, and assume the following values for a simple beam with uniform thickness.

a	12	*e*	1.2	*i*	-0.6	*r*	1/700
b	4	*g*	2/15	*j*	-1/15	*s*	11/6300
c	-6	*h*	-0.1	*k*	1/20	*q*	-1/1400

Table 1. Stiffness, Kinematic and Elastokinematic Coefficients for a Simple Beam

In general, these coefficients are functionals of the beam's spatial thickness function *t(X)*. A quantification of these coefficients in terms of the beam shape provides the basis for a sensitivity analysis and shape optimization. The particular shape variation illustrated in Fig. 2 is discussed in further detail, later in this section.

The maximum estimated error in the analysis so far is less than *5%* for transverse displacements within ± *0.1* and axial force within ± *10*. Unlike the original results (1) and (3), expressions (7)-(8) express the role of the normalized axial force $\boldsymbol{p}$ in the force-displacement relations of the beam in a simple matrix format. The two components of transverse stiffness, commonly referred to as the elastic stiffness matrix and the geometric stiffness matrix, are clearly quantified in expression (7). This characterizes the load-stiffening effect in a beam, and consequently the loss in the quality of DOF in the presence of a tensile axial force. Of particular interest is the change in axial stiffness in the presence of a transverse displacement, as evident in expression (8). It may be seen that the kinematic component defined earlier may be further separated into a purely kinematic component, and an *elastokinematic* component. The latter is named so because of its dependence on the axial force as well as the kinematic requirement of constant beam arc-length. This component essentially captures the effect of the change in the beam's deformed shape due to the axial force, for given transverse displacements. Since this term contributes additional compliance along the axial direction, it compromises the quality of the *x* DOC. For an applied force $\boldsymbol{f}$, the displacement *x* and rotation θ are undesired. Since these correspond to a DOC and DOF respectively, any *x* displacement is a parasitic error motion and θ rotation is a cross-axis error motion. While the latter is explicitly load-dependent and can be eliminated by an appropriate combination of the transverse loads $\boldsymbol{f}$ and $\boldsymbol{m}$, the former has kinematic as well as elastokinematic components and therefore cannot be entirely eliminated.

These observations are significant because they parametrically illustrate the role of the force along a DOC on the quality of DOF due to load-stiffening. Furthermore, the range of motion along DOF is limited to ensure an acceptably small stiffness reduction and error motion along

the DOC due to elastokinematic effects. These are the classic tradeoffs in flexure performance, and are not captured in a traditional linear analysis.

The accuracy of the above derivations may be verified using known cases of beam buckling, as long as the magnitude of the corresponding normalized buckling loads is less than *10*. Buckling limit corresponds to the compressive load at which the transverse stiffness of a beam becomes zero. Using this definition and expression (4) for a fixed-free beam, one can estimate the buckling load to be $\boldsymbol{p}_{crit} = -2.5$, which is less than *1.3%* off from the classical beam buckling prediction of $\boldsymbol{p}_{crit} = -\pi^2/4$. Similarly, the buckling load for a beam with zero end slopes is predicted to be -10 using expression (5), as compared to $-\pi^2$ derived using the classical theory. Many other non-trivial results may be easily derived from the proposed simplified expressions, using appropriate boundary conditions. For example, in the presence of an axial load $\boldsymbol{p}$, the ratio between $\boldsymbol{m}$ and $\boldsymbol{f}$ required to ensure zero beam-end rotation is given by $-\left(1+\frac{1}{60}\boldsymbol{p}\right)/2\left(1+\frac{1}{10}\boldsymbol{p}\right)$, which determines the COS of the beam with respect to the beam-end and force $\boldsymbol{f}$. An example that illustrates a design tradeoff is that of a clamped-clamped beam of actual length *2L* transversely loaded in the center. While symmetry ensures perfect straight-line motion along the *y* DOF, and no error motions along *x* or θ, it also results in a non-linear stiffening effect along the DOF given by $\boldsymbol{f} = 2(a - i\,d\,e\,y^2)y$, which significantly limits the range of allowable motion. This non-linear stiffness behavior is derived in a few steps from expressions (7)-(8), whereas the conventional methods can be considerably more time-consuming.

Next, we consider the specific generalization of beam geometry shown in Fig. 2. The non-linear force-displacement relationships for this beam geometry may be obtained mathematically by treating the two end-segments as simple beams, and using the prior results of this section.

$$\begin{bmatrix}\boldsymbol{f}\\ \boldsymbol{m}\end{bmatrix} \approx \frac{1}{\left(3-6a_o+4a_o^2\right)a_o}\begin{bmatrix}6 & -3\\ -3 & 3-3a_o+2a_o^2\end{bmatrix}\begin{bmatrix}y\\ \theta\end{bmatrix} + \frac{\boldsymbol{p}}{5\left(3-6a_o+4a_o^2\right)^2}\begin{bmatrix}3\left(15-50a_o+60a_o^2-24a_o^3\right) & -a_o\left(15-60a_o+84a_o^2-40a_o^3\right)\\ -a_o\left(15-60a_o+84a_o^2-40a_o^3\right) & a_o\left(15-60a_o+92a_o^2-60a_o^3+\frac{40}{3}a_o^4\right)\end{bmatrix}\begin{bmatrix}y\\ \theta\end{bmatrix} \tag{9}$$

$$x = 2a_o\left(\frac{t^2}{12}\right)\boldsymbol{p} + \frac{\begin{bmatrix} y & \theta \end{bmatrix}}{10\left(3-6a_o+4a_o^2\right)^2}\begin{bmatrix} -3\left(15-50a_o+60a_o^2-24a_o^3\right) & a_o\left(15-60a_o+84a_o^2-40a_o^3\right) \\ a_o\left(15-60a_o+84a_o^2-40a_o^3\right) & -a_o\left(15-60a_o+92a_o^2-60a_o^3+\frac{40}{3}a_o^4\right) \end{bmatrix}\begin{bmatrix} y \\ \theta \end{bmatrix}$$

$$+\boldsymbol{p}\frac{a_o^3\begin{bmatrix} y & \theta \end{bmatrix}}{175\left(3-6a_o+4a_o^2\right)^3}\begin{bmatrix} 2\left(105-630a_o+1440a_o^2-1480a_o^3+576a_o^4\right) & -\left(105-630a_o+1440a_o^2-1480a_o^3+576a_o^4\right) \\ -\left(105-630a_o+1440a_o^2-1480a_o^3+576a_o^4\right) & \left(105-630a_o+1560a_o^2-2000a_o^3+1408a_o^4-560a_o^5+\frac{1120}{9}a_o^6\right) \end{bmatrix}\begin{bmatrix} y \\ \theta \end{bmatrix}$$

(10)

It is significant to note that these force-displacement relations are of the same matrix equation format as expressions (7)-(8). Obviously, the transverse direction elastic and geometric stiffness coefficients are now functions of a_o, a non-dimensional number. As expected, for a fixed beam thickness, reducing the length of the end-segments increases the elastic stiffness, while reducing the geometric stiffness. In the limiting case of $a_o \rightarrow 0$, which corresponds to a lumped-compliance topology, the elastic stiffness becomes infinitely large, and the first geometric stiffness coefficient reduces to *1* while the others vanish. Similarly, the axial direction elastic stiffness as well as the kinematic and elastokinematic coefficients are also functions of beam segment length a_o. In the limiting case of $a_o \rightarrow 0$, the elastic stiffness becomes infinitely large, the first kinematic coefficient approaches *0.5*, and the remaining kinematic coefficients along with all the elastokinematic coefficients vanish. This simply reaffirms the prior observation that elastokinematic effects are a consequence of distributed compliance. For the other extreme of $a_o \rightarrow 0.5$, which corresponds to a simple beam, it may be verified that the above transverse elastic and geometric stiffness coefficients, and the axial elastic stiffness, kinematic and elastokinematic coefficients take the numerical values listed earlier in Table 1.

Observations on these two limiting cases agree with the common knowledge and physical understanding of distributed-compliance and lumped-compliance topologies. Significantly, expressions (9)-(10) provide an analytical comparison of these two limiting case topologies, and those in between. To graphically illustrate the effect of distribution of compliance, the stiffness and constraint coefficients are plotted as functions of length parameter a_o in Figures 4 through 8. Assuming a certain beam thickness limited by the maximum allowable axial stress, one topology extreme, $a_o = 0.5$, provides the lowest elastic stiffness along the *y* DOF (Fig. 4), and therefore is best suited to maximize the primary motion. However, this is prone to moderately higher load-stiffening behavior, as indicated by the geometric stiffness coefficients in Fig. 5, and parasitic errors along the *x* DOC, as indicated by the kinematic coefficients in Fig. 6. Most importantly,

this topology results in the highest elastokinematic coefficients plotted in Fig. 7, which compromise the stiffness and error motions along the x DOC, but at the same time make this topology best suited for approximate-constraint design. Approaching the other topology extreme, $a_o \rightarrow 0$, there are gains on several fronts. Elastic stiffness along the x DOC improves (Fig. 8), stress-stiffening effects decrease (Fig. 5), kinematic effects diminish or vanish (Fig. 6), and elastokinematic effects are entirely eliminated (Fig. 7). However, these advantages are achieved at the expense of an increased stiffness along the transverse direction, which limits the primary motion for a given maximum allowable bending stress. It may be observed that of all the beam characteristic coefficients, only the normalized axial stiffness is dependent on the beam thickness. A value of $t = 1/50$ is assumed in Fig. 8.

Thus, once again we are faced with performance trade-offs in flexure geometry design. The significance of the closed-form results (9)-(10) is that for given stiffness and error motion requirements in an application, an optimal beam topology, somewhere between the two extremes, may be easily selected. For example, $a_o = 0.2$ provides a beam topology that has *150%* higher axial stiffness, *78%* lower elastokinematic effects, *6%* lower stress-stiffening and kinematic effects, at the expense of a *27%* increase in the primary direction stiffness.

It is important to note that as the parameter a_o becomes small, Bernoulli's assumptions are no longer accurate and corrections based on Timoshenko's beam theory may be readily incorporated in the above analysis. However, the strength of this formulation is the illustration that irrespective of the beam's shape, its nonlinear force-displacement relationships, which eventually determine its performance characteristics as a flexure constraint, can always be captured in a consistent matrix based format with variable non-dimensional coefficients. Beams with even further generalized geometries such as continuously varying thickness may be similarly modeled. As mentioned earlier, this provides an ideal basis for a shape sensitivity and optimization study. In all the subsequent flexure modules considered in this paper, although the figures show simple beam flexure elements, the presented analysis holds true for any generalized beam shape.

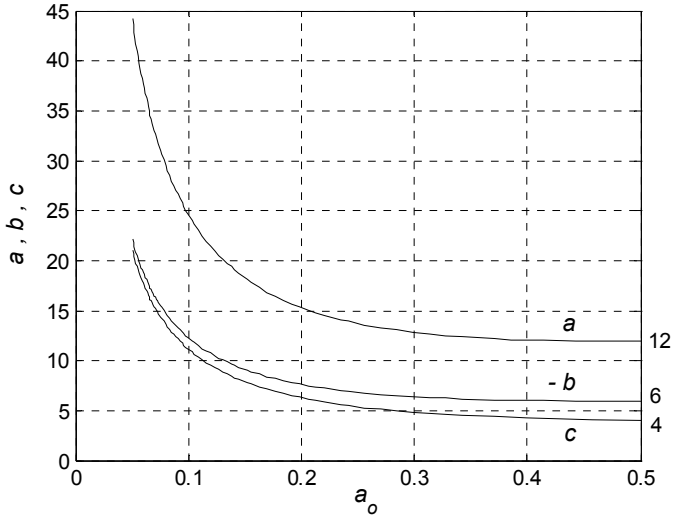

Fig.4 Transverse Elastic Stiffness Coefficients

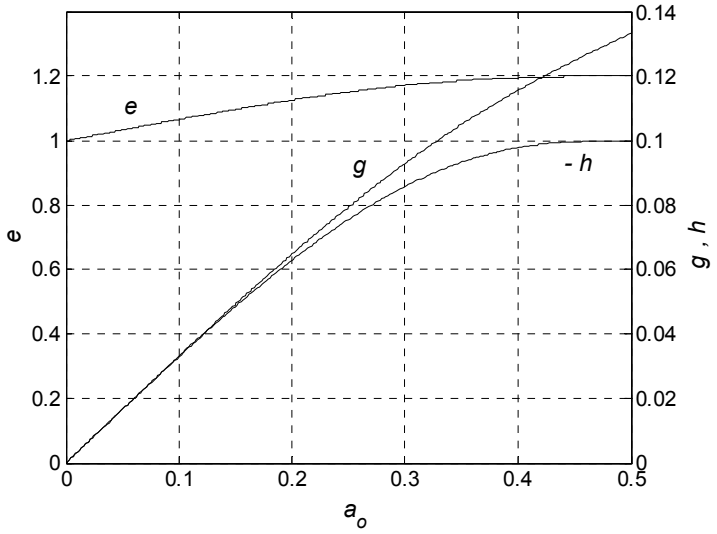

Fig.5 Transverse Geometric Stiffness Coefficients

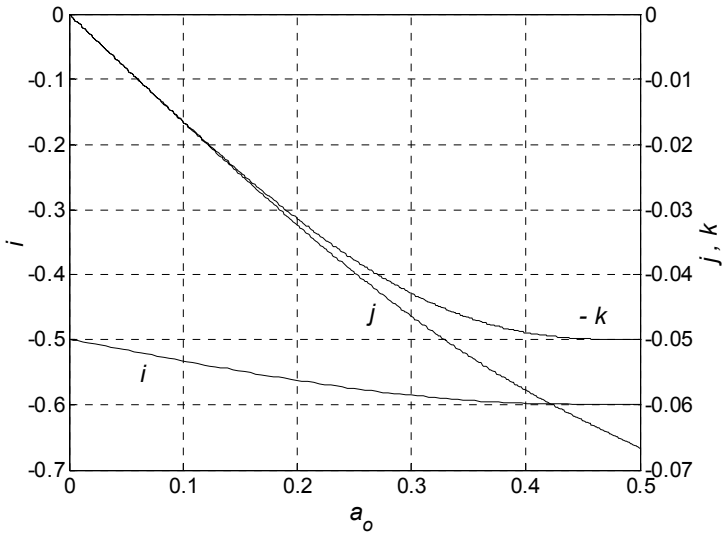

Fig.6 Axial Kinematic Coefficients

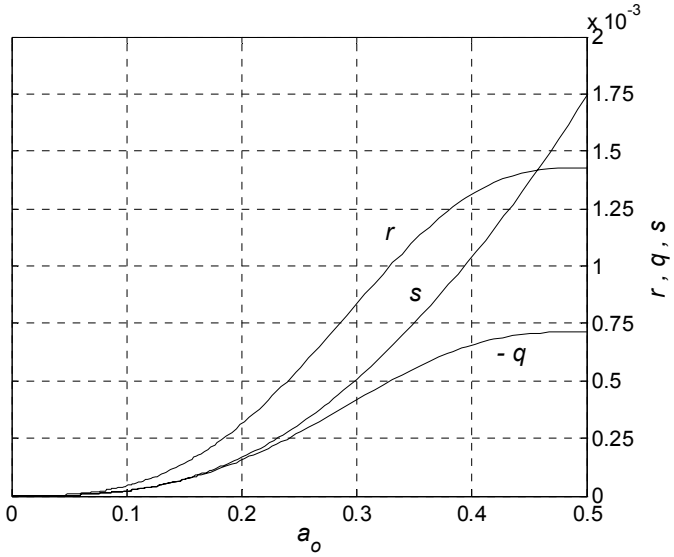

Fig.7 Axial Elastokinematic Coefficients

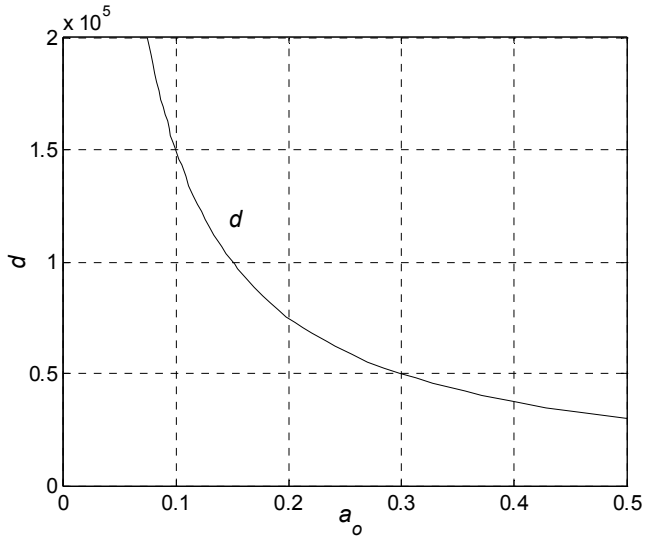

Fig.8 Axial Elastic Stiffness Coefficient

4. Parallelogram Flexure and Variations

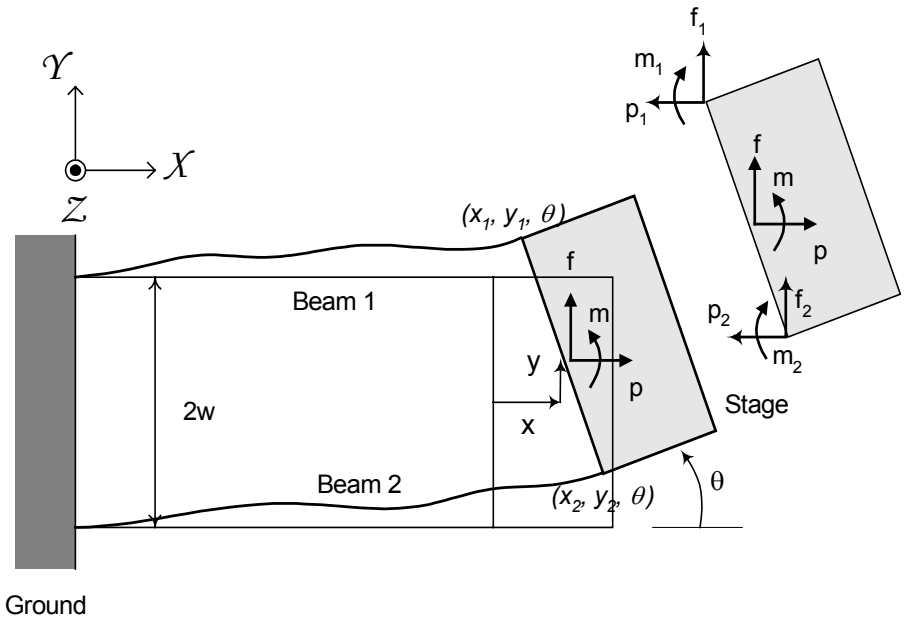

Fig.9 Parallelogram Flexure and Stage Free Body Diagram

The parallelogram flexure, shown in Fig. 9, provides a constraint arrangement that allows approximate straight-line motion. The *y* displacement represents a DOF, while *x* and θ are DOC. The two beams are treated as perfectly parallel and identical, at least initially, and the stage connecting these two is assumed rigid. Loads and displacements can be normalized with respect

to the properties of either beam. Linear analysis of the parallelogram flexure module, along with the kinematic requirement of constant beam arc-length, yields the following standard results [3].

$$\begin{bmatrix} \boldsymbol{f} \\ \boldsymbol{m} \end{bmatrix} = 2\begin{bmatrix} a & c \\ c & w^2 d + b \end{bmatrix}\begin{bmatrix} y \\ \theta \end{bmatrix} \approx 2\begin{bmatrix} a & c \\ c & w^2 d \end{bmatrix}\begin{bmatrix} y \\ \theta \end{bmatrix}$$
$$x \approx \frac{\boldsymbol{p}}{2d} + iy^2 \tag{11}$$

The above approximations are based on the fact that elastic axial stiffness d is at least four orders of magnitude larger than elastic transverse stiffness a, b and c, for typical dimensions and beam shapes. Based on this linear analysis, stage rotation θ can be shown to be several orders of magnitude smaller than the y displacement. However, our objective here is to determine the more representative non-linear force-displacement relations for the parallelogram flexure. Conditions of geometric compatibility yield,

$$x = \frac{(x_1^e + x_2^e)}{2} + \frac{(x_1^k + x_2^k)}{2} \triangleq x^e + x^k$$
$$w\theta = \frac{(x_2^e - x_1^e)}{2} + \frac{(x_2^k - x_1^k)}{2} \tag{12}$$
$$y_1 = y - \frac{w\theta^2}{2} \quad ; \quad y_2 = y + \frac{w\theta^2}{2} \quad \Rightarrow \quad y_1 \approx y_2 \approx y$$

Force equilibrium conditions are derived from the Free Body Diagram of the stage in Fig. 9. While force equilibrium is applied in a deformed configuration to capture non-linear effects, the contribution of θ is negligible.

$$\boldsymbol{p}_1 + \boldsymbol{p}_2 = \boldsymbol{p} \quad ; \quad \boldsymbol{f}_1 + \boldsymbol{f}_2 = \boldsymbol{f} \quad ; \quad \boldsymbol{m}_1 + \boldsymbol{m}_2 + (\boldsymbol{p}_2 - \boldsymbol{p}_1)w = \boldsymbol{m} \tag{13}$$

These geometric compatibility and force equilibrium conditions, along with force-displacement results (7)-(8) applied to each beam, yield

$$\boldsymbol{f} = \boldsymbol{f}_1 + \boldsymbol{f}_2 = (2a + \boldsymbol{p}e)y + (2c + \boldsymbol{p}h)\theta$$
$$\boldsymbol{m}_1 + \boldsymbol{m}_2 = (2c + \boldsymbol{p}h)y + (2b + \boldsymbol{p}g)\theta$$
$$x^e = \frac{1}{2d}(\boldsymbol{p}_1 + \boldsymbol{p}_2) \quad ; \quad x^k = \begin{bmatrix} y & \theta \end{bmatrix}\begin{bmatrix} i & k \\ k & j \end{bmatrix}\begin{bmatrix} y \\ \theta \end{bmatrix} + \frac{(\boldsymbol{p}_1 + \boldsymbol{p}_2)}{2}\begin{bmatrix} y & \theta \end{bmatrix}\begin{bmatrix} r & q \\ q & s \end{bmatrix}\begin{bmatrix} y \\ \theta \end{bmatrix} \tag{14}$$
$$\theta = \left\{ \frac{1}{d} + \begin{bmatrix} y & \theta \end{bmatrix}\begin{bmatrix} r & q \\ q & s \end{bmatrix}\begin{bmatrix} y \\ \theta \end{bmatrix} \right\} \cdot \left\{ \frac{\boldsymbol{m} - (2c + \boldsymbol{p}h)y - (2b + \boldsymbol{p}g)\theta}{2w^2} \right\}$$

Unlike in the linear analysis, it is important to recognize that neither $\boldsymbol{f_1}$ and $\boldsymbol{f_2}$, nor $\boldsymbol{m_1}$ and $\boldsymbol{m_2}$, are equal despite the fact that the transverse displacements, y and θ, for the two beams are constrained to be the same. This is due to the different values of axial forces $\boldsymbol{p_1}$ and $\boldsymbol{p_2}$, which result in unequal transverse stiffness changes in the two beams. Shifting attention to the expression for θ above, the first term represents the consequence of elastic contraction and stretching of the top and bottom beams, respectively. The second term, which is rarely accounted for in the literature, is the consequence of the elastokinematic effect explained in the previous section. Since the axial forces on the two beams are unequal, apart from resulting in different elastic deflections of the two beams, they also cause slightly different beam shapes and therefore different elastokinematic axial deflections. Because of its linear dependence on the axial load and quadratic dependence on the transverse displacement, this elastokinematic effect contributes a non-linear component to the stage rotation. The purely kinematic part of the axial deflection of the beams is independent of the axial force, and therefore does not contribute to θ. However, it does contribute to the stage axial displacement x, which also comprises of a purely elastic component and an elastokinematic component. Using equations (12)-(14), one can now solve the force-displacement relationships of the parallelogram flexure. For simplification, higher order terms of θ are dropped wherever appropriate.

$$\theta = \frac{\left(4a^2 + 4\boldsymbol{p}ea + \boldsymbol{p}^2e^2 + \boldsymbol{f}^2dr\right)\left(2\boldsymbol{m}a - 2\boldsymbol{f}c + \boldsymbol{p}(me - \boldsymbol{f}h)\right)}{2w^2d(2a + e\boldsymbol{p})^3} = \frac{1}{2w^2}\left(\frac{1}{d} + y^2r\right)\left[\boldsymbol{m} - y\left(2c + \boldsymbol{p}h\right)\right] \quad (15)$$

$$y = \frac{\boldsymbol{f} - \left(2c + \boldsymbol{p}h\right)\theta}{\left(2a + \boldsymbol{p}e\right)} = \frac{\boldsymbol{f}}{\left(2a + \boldsymbol{p}e\right)} - \frac{\left(2c + \boldsymbol{p}h\right)}{2w^2\left(2a + \boldsymbol{p}e\right)}\left(\frac{1}{d} + \frac{\boldsymbol{f}^2r}{\left(2a + \boldsymbol{p}e\right)^2}\right)\left(\boldsymbol{m} - \boldsymbol{f}\frac{\left(2c + \boldsymbol{p}h\right)}{\left(2a + \boldsymbol{p}e\right)}\right) \approx \frac{\boldsymbol{f}}{\left(2a + \boldsymbol{p}e\right)} \quad (16)$$

$$x \approx \frac{\boldsymbol{p}}{2d} + y^2i + \frac{\boldsymbol{p}}{2}y^2r \quad (17)$$

Assuming uniform thickness beams, with nominal dimensions of $t=1/50$ and $w=3/10$, parallelogram flexure force-displacement relations based on the linear and non-linear closed-form analyses (CFA), and non-linear Finite Element Analysis (FEA) are plotted in Figures 10 through 13. The inadequacy of the traditional linear analysis is evident in Fig. 10, which plots the stage rotation using expression (15). The non-linear component of stage rotation derived from the relative elastokinematic axial deflections of the two beams increases with a compressive

axial load $\boldsymbol{p}$. Since the stage rotation is undesirable in response to the transverse force $\boldsymbol{f}$, it is a parasitic error motion comprising of elastic and elastokinematic components, and may therefore be eliminated by an appropriate combination of transverse loads. In fact, the COS location for the parallelogram module is simply given by the ratio between $\boldsymbol{m}$ and $\boldsymbol{f}$ that makes the stage rotation zero. This ratio is easily calculated from (15) to be $\left(2c+\boldsymbol{p}h\right)/\left(2a+\boldsymbol{p}e\right)$, and is equal to -0.5 in the absence of an axial load, which agrees with common knowledge.

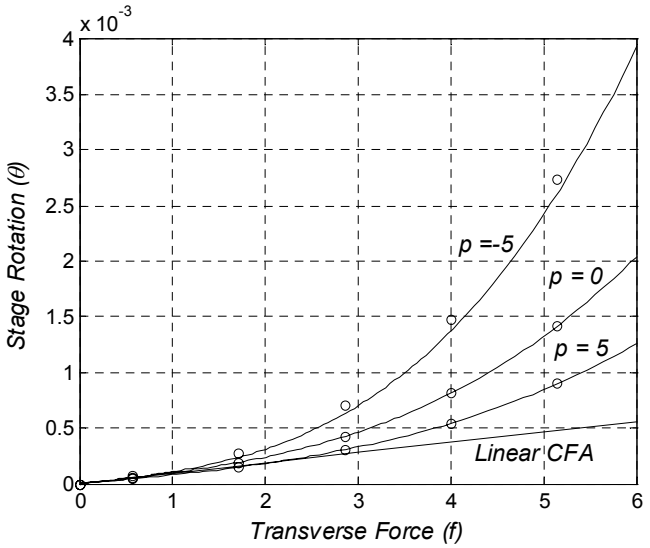

Fig.10 Parallelogram Flexure Stage Rotation: CFA (Lines), FEA (Circles)

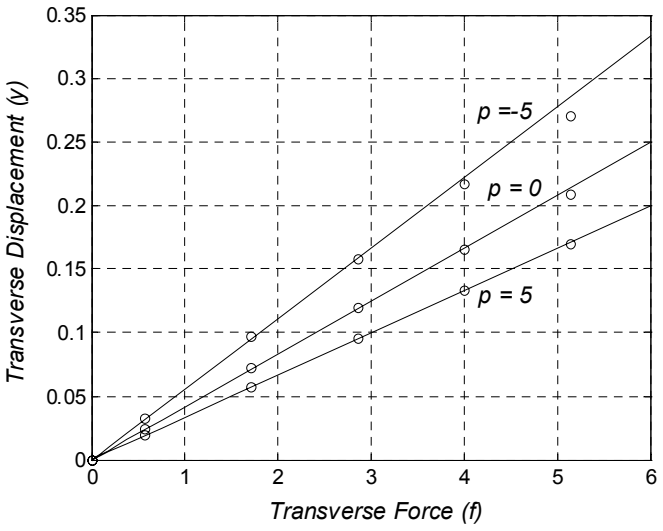

Fig.11 Parallelogram Flexure Transverse Displacement: CFA (Lines), FEA (Circles)

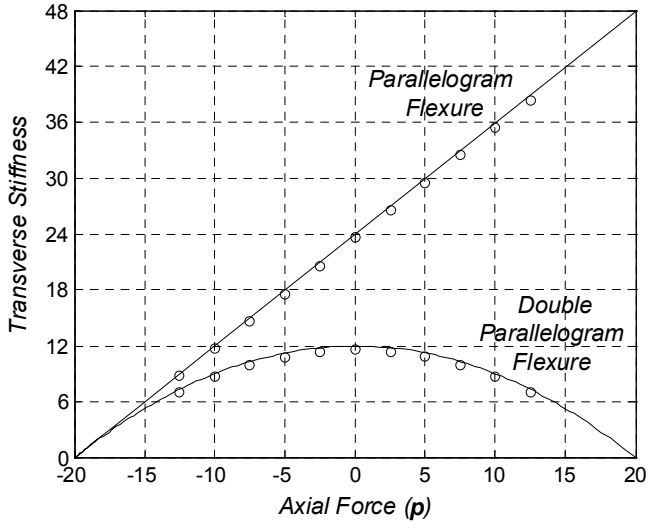

Fig.12 Parallelogram and Double Parallelogram Flexures Transverse Stiffness: CFA (Lines), FEA (Circles)

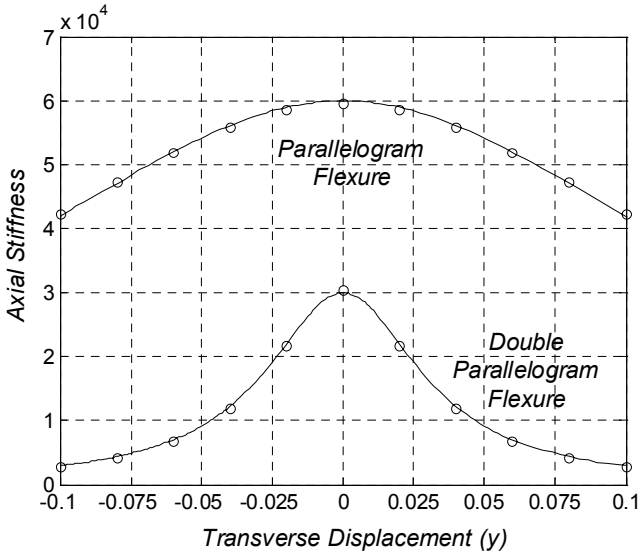

Fig.13 Parallelogram and Double Parallelogram Flexures Axial Stiffness: CFA (Lines), FEA (Circles)

Expression (16) describes the transverse force displacement behavior of the parallelogram flexure, which is plotted in Figures 11 and 12. Since θ is several orders smaller than y, its contribution in this expression is generally negligible and may be dropped. This effectively results in a decoupling between the transverse moment $\boldsymbol{m}$ and displacement y. However, it should be recognized that since θ is dependent on $\boldsymbol{f}$, reciprocity does require y to be dependent on $\boldsymbol{m}$, which becomes important only in specific cases, for example, when the transverse end load is a pure moment. Thus, the relation between $\boldsymbol{f}$ and y is predominantly linear. As shown in Fig. 12, the transverse stiffness has a linear dependence on the axial force, and approaches zero for $p = -20$, which physically corresponds to the condition for buckling.

The axial force-displacement behavior is given by expression (17), which also quantifies the dependence of axial compliance on transverse displacements. Axial stiffness drops quadratically with y and the rate of this drop depends on the coefficient r, which is $1/700$ for a simple beam. For a typical case when $t=1/50$, the axial stiffness reduces by about 30% for a transverse displacement y of 0.1, as shown in Fig. 13. Based on the error motion characterization in Section 2, any x displacement will be a parasitic error motion, which in this case comprises of elastic, purely kinematic as well as elastokinematic components. The kinematic component, being a few orders of magnitude higher than the others and determined by $i = -0.6$, dominates the error motion. The stiffness and error motion along the X direction represent the quality of DOC of the parallelogram module, and influence its suitability as a flexure building block. This module may be mirrored about the motion stage, so that the resulting symmetry eliminates any x or θ error motions in response to a primary y motion, and improves the stiffness along these DOC directions. However, this attempt to improve the quality of DOC results in a non-linear stiffening of the DOF direction, leading to over-constraint.

Next, a sensitivity analysis may be performed to determine the effect of differences between the two beams in terms of material, shape, thickness, length or separation. For the sake of illustration, a parallelogram flexure with beams of unequal lengths, L_1 and L_2, is considered. L_1 is used as the characteristic length in the mechanism and error metric Δ is defined to be $(1-L_2/L_1)$. Force-displacement relationships for Beam 1 remain the same as earlier (7)-(8), whereas those for Beam 2 change as follows, for small Δ.

$$\begin{bmatrix} \boldsymbol{f_2} \\ \boldsymbol{m_2} \end{bmatrix} = \begin{bmatrix} (1+3\Delta)a & (1+2\Delta)c \\ (1+2\Delta)c & (1+\Delta)b \end{bmatrix} \begin{bmatrix} y \\ \theta \end{bmatrix} + \boldsymbol{p_2} \begin{bmatrix} (1+\Delta)e & h \\ h & (1-\Delta)g \end{bmatrix} \begin{bmatrix} y \\ \theta \end{bmatrix} \tag{18}$$

$$\begin{aligned} x_2^e &= \frac{(1-\Delta)}{d}\boldsymbol{p_2} \\ x_2^k &= \begin{bmatrix} y & \theta \end{bmatrix} \begin{bmatrix} (1+\Delta)i & k \\ k & (1-\Delta)j \end{bmatrix} \begin{bmatrix} y \\ \theta \end{bmatrix} + \boldsymbol{p_2} \begin{bmatrix} y & \theta \end{bmatrix} \begin{bmatrix} (1-\Delta)r & (1-2\Delta)q \\ (1-2\Delta)q & (1-3\Delta)s \end{bmatrix} \begin{bmatrix} y \\ \theta \end{bmatrix} \end{aligned} \tag{19}$$

Conditions of geometric compatibility (12) and force equilibrium (13) remain the same. These equations may be solved simultaneously, which results in the following stage rotation for the specific case of $\boldsymbol{m}=\boldsymbol{p}=0$.

$$\theta = \frac{x_2 - x_1}{2w} \approx -\frac{c\ (1+\Delta)(2-\Delta)}{2w^2}\left(\frac{y}{d} + ry^3\right) + \frac{iy^2}{2w}\Delta \tag{20}$$

Setting $\Delta=0$ obviously reduces this to the stage rotation for the ideal case (15). It may be noticed that unequal beam lengths result in an additional term in the stage rotation, which has a quadratic dependence on the transverse displacement y. This arises due to the purely kinematic axial displacement components of the two beams that cancelled each other in the case of identical beams. The prediction of expression (20) is plotted in Fig. 14 assuming simple beams, $t=1/50$, $w=3/10$, and two cases of Δ, along with FEA results.

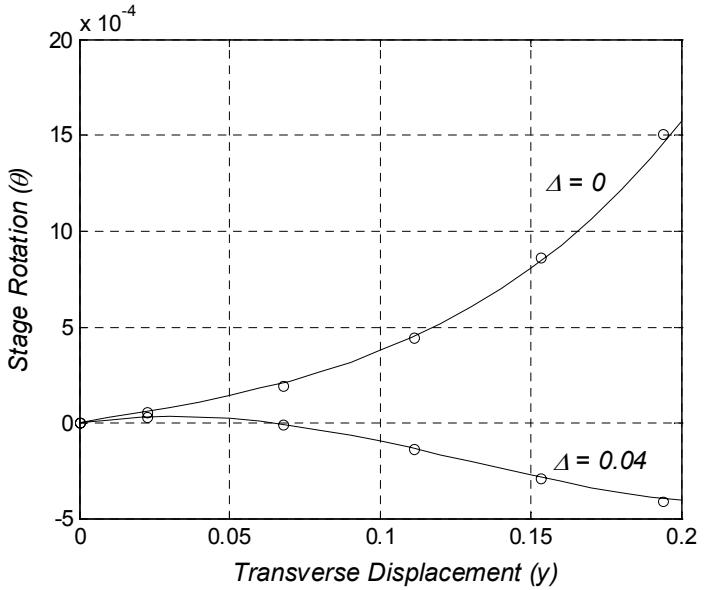

Fig.14 'Non-identical Beam' Parallelogram Flexure Stage Rotation: CFA (Lines), FEA (Circles)

Any other differences in the two parallel beams in terms of thickness, shape, or material may be similarly modeled and their effect on the characteristics of the parallelogram flexure accurately predicted. An important observation in this particular case is that an understanding of the influence of Δ on the stage rotation may be used to an advantage. If in a certain application the center of stiffness of the parallelogram flexure is inaccessible, a pre-determined discrepancy in the parallelogram geometry may be deliberately introduced to considerably reduce the stage rotation, as observed in Fig. 14. For a given range of y motion, Δ may be optimized to place a limit on maximum possible stage rotation, without having to move the transverse force application point to the COS.

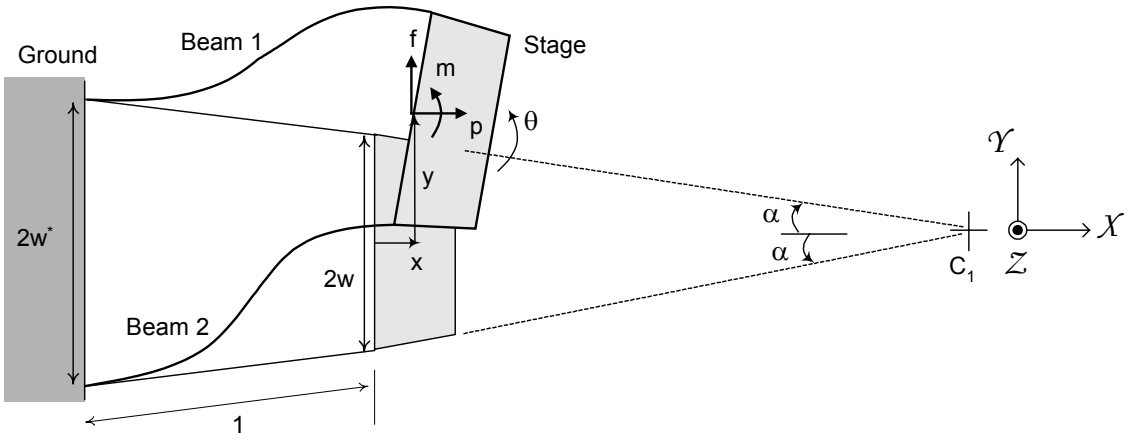

Fig.15 Tilted-beam Flexure

Another important variation of the parallelogram flexure is the tilted-beam flexure, in which case the two beams are not perfectly parallel, as shown in Fig. 15. This may result either due to poor manufacturing and assembly tolerances, or because of an intentional design to achieve a remote center of rotation at C_1. Assuming a symmetric geometry about the X-axis and repeating an analysis similar to the previous two cases, the following non-linear force-displacement results are obtained for this flexure module.

$$\theta \approx \frac{l}{2w^2\cos\alpha}\left[\boldsymbol{m} - \left(2\bar{c} + \bar{h}\frac{\boldsymbol{p}}{\cos\alpha}\right)\frac{y}{\cos\alpha}\right]\left[\frac{l}{d} + \left(\frac{y}{\cos\alpha}\right)^2 \bar{r}\right] - \frac{y\alpha}{w} \tag{21}$$

$$y \approx \frac{\left(\boldsymbol{f} \cos\alpha - \boldsymbol{m} \frac{\alpha}{w} \right)}{\left(2\overline{a} + \frac{\boldsymbol{p}}{\cos\alpha} \overline{e} \right)} \tag{22}$$

$$x \approx \frac{\boldsymbol{p}}{2d\cos^2\alpha} + \frac{y^2}{\cos^3\alpha}\left(\overline{i} + \frac{\boldsymbol{p}}{2\cos\alpha} \overline{r} \right) \tag{23}$$

The newly introduced dimensionless coefficients $\overline{a}$, $\overline{c}$, $\overline{e}$, $\overline{h}$, $\overline{i}$ and $\overline{r}$ are related to the original beam characteristic coefficients along with the geometric parameter α, as follows.

$$\begin{aligned} &\overline{a} = \left(a - \frac{2c}{w}\alpha + \frac{a}{2}\alpha^2 + \frac{b}{w^2}\alpha^2 \right) \quad ; \quad \overline{e} \triangleq \left(e - \frac{2h}{w}\alpha + \frac{e}{2}\alpha^2 + \frac{g}{w^2}\alpha^2 \right) \\ &\overline{c} \triangleq \left(c - aw\alpha - b\frac{\alpha}{w} + c\alpha^2 \right) \quad ; \quad \overline{h} \triangleq \left(h - ew\alpha - g\frac{\alpha}{w} + h\alpha^2 \right) \\ &\overline{i} \triangleq \left(i - 2k\frac{\alpha}{w} + j\frac{\alpha^2}{w^2} \right) \quad ; \quad \overline{r} \triangleq \left(r - 2q\frac{\alpha}{w} + s\frac{\alpha^2}{w^2} \right) \end{aligned} \tag{24}$$

These derivations are made assuming small values of α of the order of *0.1*, and readily reduce to expressions (15)-(17) for $\alpha = 0$. The most important observation based on expression (21) is that unlike the ideal parallelogram flexure, the stage rotation θ has an additional linear kinematic dependence on the primary motion y, irrespective of the loads. This kinematic dependence dominates the stage rotation for typical values of α of the order of *0.1*. This implies that, as a consequence of the tilted beam configuration, the motion stage has an approximate Virtual Center of Rotation located at C_1. It should be noted that the Virtual Center of Rotation and Center of Stiffness are fundamentally distinct concepts. The former represents a point in space about which a certain stage in a mechanism rotates upon the application of a certain allowable force, whereas the latter represents that particular location on this stage where the application of the said allowable force produces no rotation. In general, the location of the Virtual Center of Rotation depends on the geometry of the mechanism and the location of the allowable force.

The magnitude of θ in this case is only a single order less than that of y, as opposed to the several orders in the ideal parallelogram. Consequently θ has not been neglected in the derivation of the above results. If transverse displacement y is the only desired motion then stage rotation θ is a parasitic error motion, comprising an elastic, elastokinematic and a dominant kinematic component.

The primary motion elastic stiffness in the tilted-beam flexure is a function of α, and the primary motion y itself has a dependence on the end-moment $\boldsymbol{m}$, as indicated by expression (22), unlike the parallelogram flexure. This coupling, which is a consequence of the tilted-beam configuration, may be beneficial if utilized appropriately, as shall be illustrated in the subsequent discussion on double tilted-beam flexure module. For a typical geometry of uniform thickness beam $t=1/50$ and $w=3/10$, and a transverse load $\boldsymbol{f} = 3$, the transverse elastic stiffness and the y-θ relation are plotted in Figures 16 and 17, respectively.

The axial displacement in this case, given by expression (23), is very similar in nature to the axial displacement of the parallelogram flexure. As earlier, x displacement represents a parasitic error motion comprising of elastic, kinematic and elastokinematic terms. Since the stage rotation is not negligible, it influences all the axial direction kinematic and elastokinematic terms. Figures 18 and 19 show the increase in the kinematic component of the axial displacement and decrease in axial stiffness, respectively, with an increasing beam tilt angle. All these factors marginally compromise the quality of the x DOC. The tilted-beam flexure is clearly not a good replacement of the parallelogram flexure if straight-line motion is desired, but is important as a virtual frictionless pivot mechanism. Quantitative results (20) and (21), regarding the stage rotation, are in perfect agreement with the empirical observations in the prior literature regarding the geometric errors in the parallelogram flexure [14].

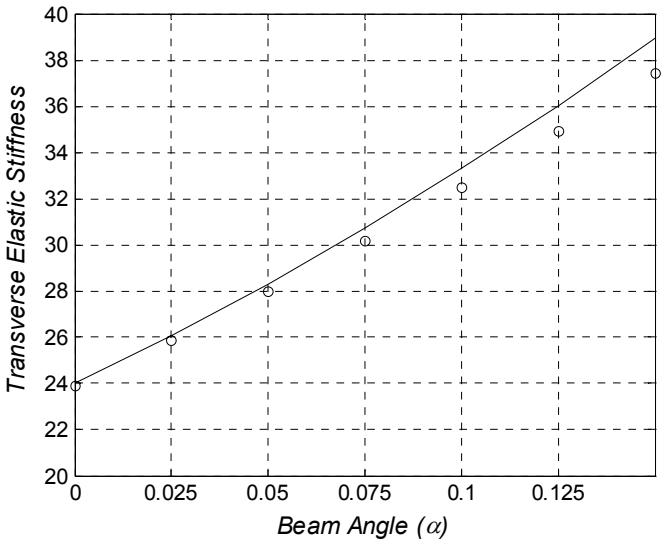

Fig.16 Tilted-beam Flexure Transverse Elastic Stiffness: CFA (Lines), FEA (Circles)

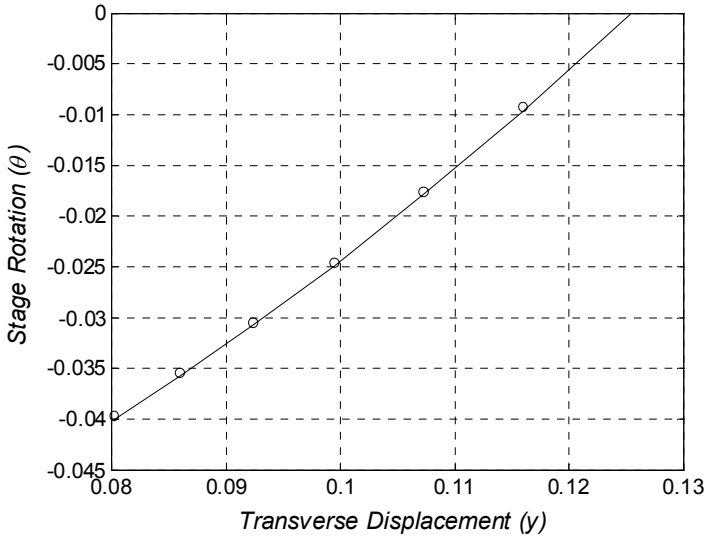

Fig.17 Tilted-beam Flexure Stage Rotation: CFA (Lines), FEA (Circles)

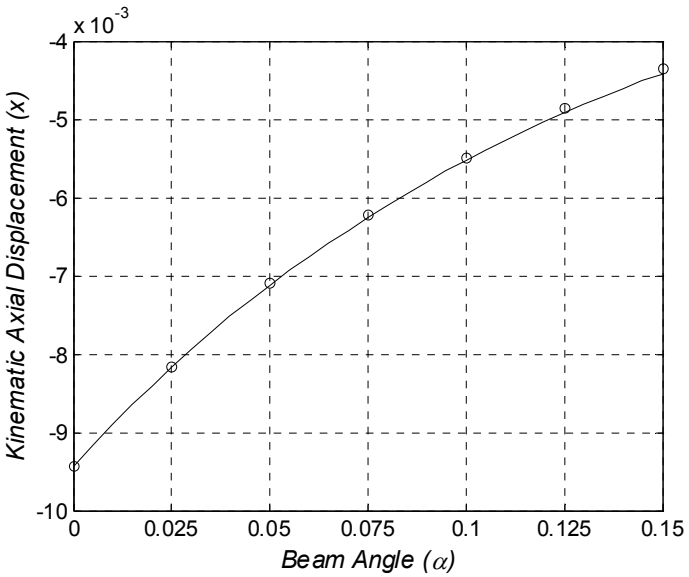

Fig.18 Tilted-beam Flexure Kinematic Axial Displacement: CFA (Lines), FEA (Circles)

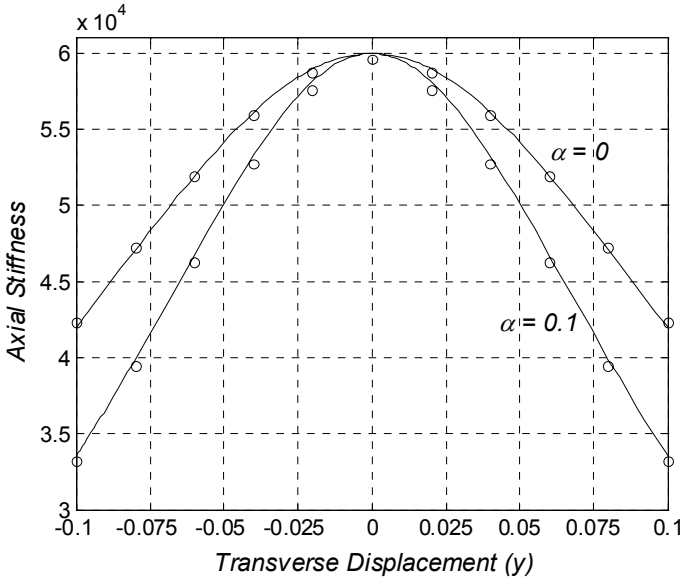

Fig.19 Tilted-beam Flexure Axial Stiffness: CFA (Lines), FEA (Circles)

5. Double Parallelogram Flexure and Variations

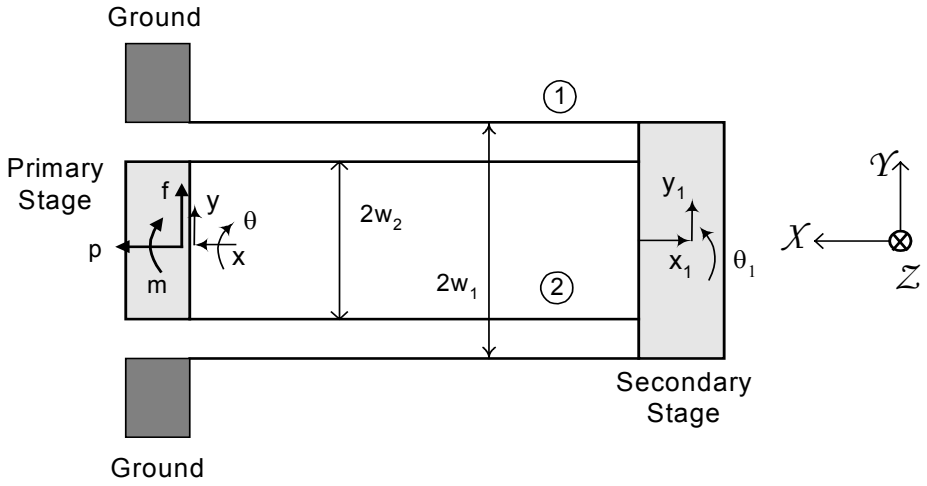

Fig.20 Double Parallelogram Flexure

The results of the previous section are easily extended to a double parallelogram flexure, illustrated in Fig. 20. The two rigid stages are referred to as the primary and secondary stages, as indicated. Loads ***f***, ***m*** and ***p*** are applied at the primary stage. The two parallelograms are treated identical, except for the beam spacing, w_1 and w_2. A linear analysis, with appropriate approximations, yields the following force-displacement relationships.

$$\begin{bmatrix} \boldsymbol{f} \\ \boldsymbol{m} \end{bmatrix} = \begin{bmatrix} a & -a/2 \\ -a/2 & \dfrac{2w_1^2 w_2^2 d}{w_1^2 + w_2^2} \end{bmatrix} \begin{bmatrix} y \\ \theta \end{bmatrix} \qquad \text{and} \qquad x = \frac{\boldsymbol{p}}{d} \tag{25}$$

To derive the non-linear force-displacement relations for this module, results (15)-(17) obtained in the previous section are applied to each of the constituent parallelograms. Geometric compatibility and force equilibrium conditions are easily obtained from Fig. 20. Solving these simultaneously while neglecting higher order terms in θ and θ_1, leads to the following results.

$$\begin{aligned} & y_1 \approx \frac{\boldsymbol{f}}{(2a - \boldsymbol{p}e)} \quad ; \quad y - y_1 \approx \frac{\boldsymbol{f}}{(2a + \boldsymbol{p}e)} \\ & \qquad \Rightarrow y = \frac{4a\boldsymbol{f}}{(2a)^2 - (e\boldsymbol{p})^2} \end{aligned} \tag{26}$$

$$\begin{aligned} & \theta_1 = \frac{1}{2w_1^2}\left(\frac{1}{d} + y_1^2 r\right)\left[\boldsymbol{m} - y_1\left(1 - \frac{\boldsymbol{p}}{(2a + ep)} + (2c - \boldsymbol{p}h)\right)\right] \quad ; \\ & \theta - \theta_1 = \frac{1}{2w_2^2}\left(\frac{1}{d} + (y - y_1)^2 r\right)\left[\boldsymbol{m} - (y - y_1)(2c + \boldsymbol{p}h)\right] \\ & \Rightarrow \theta = \frac{1}{2w_1^2}\left(\frac{1}{d} + \frac{\boldsymbol{f}^2}{(2a - \boldsymbol{p}e)^2} r\right)\left[\boldsymbol{m} - \frac{\boldsymbol{f}}{(2a - \boldsymbol{p}e)}\left(1 - \frac{\boldsymbol{p}}{(2a + ep)} + (2c - \boldsymbol{p}h)\right)\right] \\ & \qquad + \frac{1}{2w_2^2}\left(\frac{1}{d} + \frac{\boldsymbol{f}^2}{(2a + \boldsymbol{p}e)^2} r\right)\left[\boldsymbol{m} - \frac{\boldsymbol{f}}{(2a + \boldsymbol{p}e)}(2c + \boldsymbol{p}h)\right] \end{aligned} \tag{27}$$

$$\begin{aligned} & x_1 = -\frac{\boldsymbol{p}}{2d} + y_1^2\left(i - \frac{\boldsymbol{p}r}{2}\right) \quad ; \quad x + x_1 = \frac{\boldsymbol{p}}{2d} + (y - y_1)^2\left(i + \frac{\boldsymbol{p}r}{2}\right) \\ & \Rightarrow x = \frac{\boldsymbol{p}}{d} + \boldsymbol{p}y^2 \frac{r\left[(2a)^2 + (e\boldsymbol{p})^2\right] - 8aei}{(4a)^2} \end{aligned} \tag{28}$$

Similar to the parallelogram flexure, the y displacement represents a DOF while x and θ displacements represent DOC. Expression (26) describes the DOF direction force-displacement relation and does not include the weak dependence on $\boldsymbol{m}$. Unlike the parallelogram flexure, it may be seen that the primary transverse stiffness decreases quadratically with an axial load. This dependence is a consequence of the fact that one parallelogram is always in tension while the other is in compression, irrespective of the direction of the axial load. A comparison between parallelogram and double parallelogram flexure modules with uniform thickness beams is shown

in Fig. 12. Clearly, the transverse stiffness variation, particularly for small values of axial force ***p***, is significantly less in the latter.

Expression (27) for primary stage rotation θ in a double parallelogram flexure is similar in nature to the parallelogram stage rotation, but its non-linear dependence on the axial load ***p*** is more complex. In the absence of a moment load, the primary stage rotation θ is plotted against the transverse force ***f***, for different axial loads, in Fig. 21. These results are obtained for a typical geometry of uniform beam thickness $t=1/50$, $w_1=0.3$ and $w_2=0.2$. The change in the $\theta - \boldsymbol{f}$ relationship with axial forces is relatively less as compared to the parallelogram flexure because for a given axial load, one of the constituent parallelograms is in tension and the other is in compression. The increase in stiffness of the former is somewhat compensated by the reduction in stiffness of the latter, thereby reducing the overall dependence on axial force.

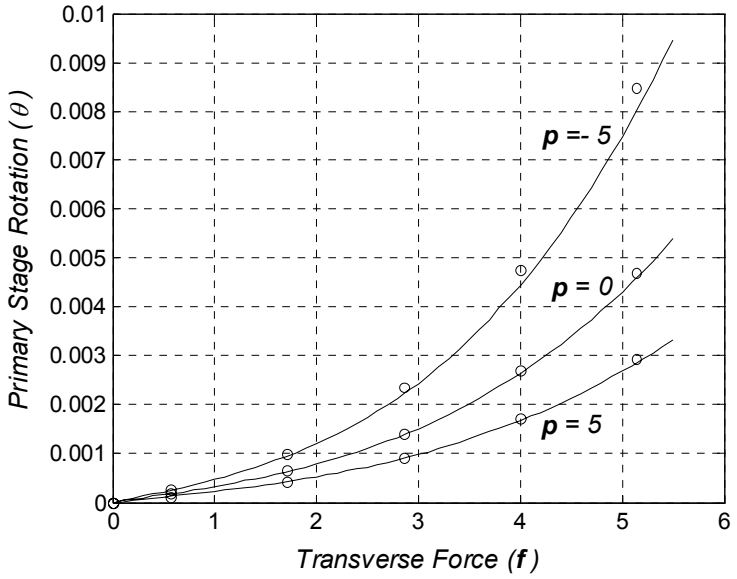

Fig.21 Double Parallelogram Flexure Primary Stage Rotation: CFA (Lines), FEA (Circles)

Since the parasitic error motion θ has elastic and elastokinematic components only, it may be entirely eliminated by appropriately relocating the transverse force ***f***, for a given ***p***. Despite the non-linear dependence of θ on transverse forces, the ***m/f*** ratio required to keep the primary stage rotation zero for ***p*** = *0*, is given by $-\dfrac{w_2^2(a+c)-w_1^2 c}{(w_2^2+w_1^2)\,a}$. For uniform thickness constituent beams, this ratio predictably reduces to – *0.5*, which then changes in the presence of an axial force.

The non-dimensional axial displacement expression (28) reveals a purely elastic term as well as an elastokinematic term, but no purely kinematic term. The purely kinematic term gets absorbed by the secondary stage due to geometric reversal. While the purely elastic term is as expected, the elastokinematic term is significantly different from the parallelogram flexure, and is not immediately obvious. The axial compliance may be further simplified as follows.

$$\frac{\partial x}{\partial \boldsymbol{p}} \approx \frac{1}{d} + \frac{y^2}{2}\left(\frac{r}{2} - \frac{ei}{a}\right) \tag{29}$$

Of the two factors that contribute elastokinematic terms, *r/2* and *ei/a*, the latter, being two orders larger than the former, dictates the axial compliance. Recalling expression (17), this *ei/a* contribution does not exist in the parallelogram flexure, and is a consequence of the double parallelogram geometry. When a *y* displacement is imposed on the primary stage, the transverse stiffness values for the two parallelograms are equal if the there is no axial load, and therefore *y* is equally distributed between the two. Referring to Fig. 20, as a tensile axial load is applied, the transverse stiffness of parallelogram 1 decreases and that of parallelogram 2 increases by the same amount, which results in a proportionate redistribution of *y* between the two as given by (26). Since the kinematic axial displacement of each parallelogram has a quadratic dependence on its respective transverse displacement, the axial displacement of parallelogram 1 exceeds that of parallelogram 2. This difference results in the unexpectedly large elastokinematic component in the axial displacement and compliance. If the axial force is compressive in nature, the scenario remains the same, except that the two parallelograms switch roles.

For the geometry considered earlier, the axial stiffness of a double parallelogram flexure is plotted against its transverse displacement *y* in Fig. 13, which shows that the axial stiffness drops by *90%* for a transverse displacement of *0.1*. This is a serious limitation in the constraint characteristics of the double parallelogram flexure module. In the transition from a parallelogram flexure to a double parallelogram flexure, while geometric reversal improves the range of motion of the DOF and eliminates the purely kinematic component of the axial displacement, it proves to be detrimental to stiffness and elastokinematic parasitic error along the *X* direction DOC.

Expressions similar to (29) have been derived previously using energy methods [11]. It has also been shown that the maximum axial stiffness can be achieved at any desired *y* location by tilting the beams of the double parallelogram flexure [15]. However, the rate at which stiffness drops

with transverse displacements does not improve because even though beams of one module are tilted with respect to the beams of the other, they remain parallel within each module. Prior literature [16] recommends the use of the double tilted-beam flexure, shown in Fig. 22, over the double parallelogram flexure to avoid a loss in axial compliance resulting from a non-rigid secondary stage, but does not discuss the above-mentioned elastokinematic effect. To really eliminate this effect, one needs to identify and address its basic source, which is the fact that the secondary stage is free to move transversely when an axial load is applied on the primary stage. Eliminating the translational DOF of the secondary stage should therefore resolve the current problem. In fact, it has been empirically suggested that an external geometric constraint be imposed on the secondary stage, for example by means of a lever arm, which requires it to have exactly half the transverse displacement of primary stage, when using a double parallelogram flexure [14]. However, this approach may lead to design complexity in terms of practical implementation.

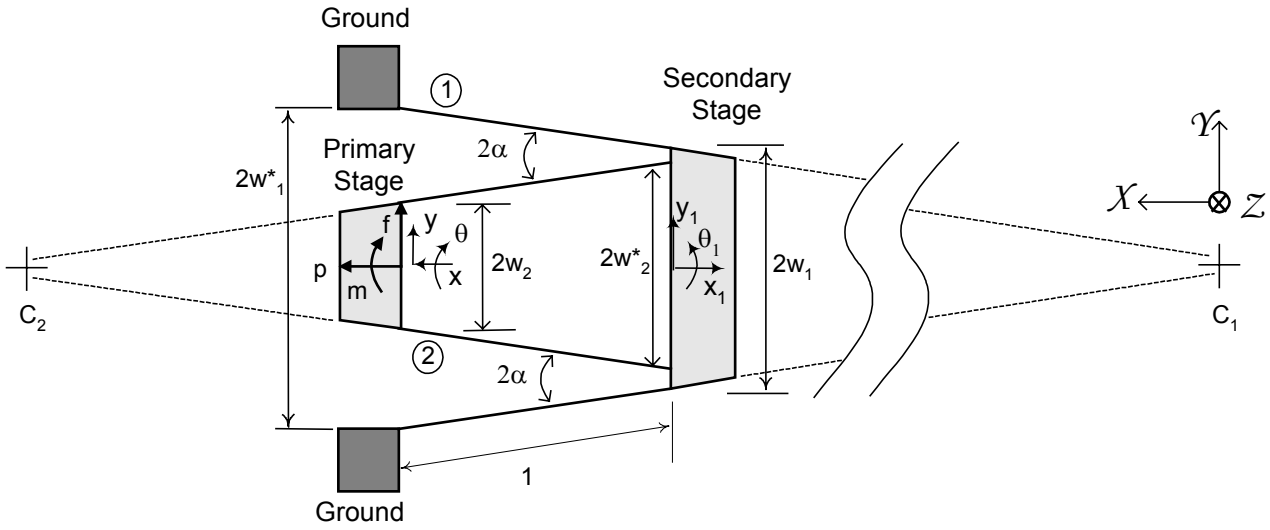

Fig.22 Double Tilted-beam Flexure

It is shown here that imposing a primary stage rotation in the double tilted-beam flexure, shown in Fig. 22, can help constrain the transverse motion of the secondary stage. Results (21)-(23) applied to the two tilted-beam flexure modules lead to the following force-displacement relations.

$$\theta_1 \approx \frac{1}{2w_1^2\cos\alpha}\left[\boldsymbol{m_1}-\left(2\bar{c}_1-\bar{h}_1\frac{\boldsymbol{p}}{\cos\alpha}\right)\frac{y_1}{\cos\alpha}\right]\left[\frac{1}{d}+\left(\frac{y_1}{\cos\alpha}\right)^2\bar{r}_1\right]-\frac{y_1\alpha}{w_1}$$

$$\theta+\theta_1 \approx -\frac{1}{2w_2^{*2}\cos\alpha}\left[\boldsymbol{m_1}+\left(2\bar{c}_2+\bar{h}_2\frac{\boldsymbol{p}}{\cos\alpha}\right)\frac{(y_1-y)}{\cos\alpha}\right]\left[\frac{1}{d}+\left(\frac{y_1-y}{\cos\alpha}\right)^2\bar{r}_2\right]+\frac{(y_1-y)\alpha}{w_2^*} \tag{30}$$

$$y_1 \approx \frac{\left(\boldsymbol{f}\cos\alpha-\boldsymbol{m_1}\frac{\alpha}{w_1}\right)}{\left(2\bar{a}_1-\frac{\boldsymbol{p}}{\cos\alpha}\bar{e}_1\right)} \quad ; \quad y_1-y \approx -\frac{\left(\boldsymbol{f}\cos\alpha+\boldsymbol{m_1}\frac{\alpha}{w_2^*}\right)}{\left(2\bar{a}_2+\frac{\boldsymbol{p}}{\cos\alpha}\bar{e}_2\right)} \tag{31}$$

In the following analysis, we assume that the primary stage rotation θ is constrained to zero, by some means. By eliminating $\boldsymbol{m_1}$, the internal moment at the secondary stage, between equations (30) and (31) the following relation between the primary and secondary transverse displacements may be derived.

$$\left[\frac{\left(2\bar{c}_1-\bar{h}_1\,\boldsymbol{p}/\cos\alpha\right)}{2w_1^2d\cos^2\alpha}+\frac{\alpha}{w_1}\right]y_1+\left[-\frac{\left(2\bar{c}_2+\bar{h}_2\,\boldsymbol{p}/\cos\alpha\right)}{2w_2^{*2}d\cos^2\alpha}+\frac{\alpha}{w_2^*}\right](y_1-y)$$
$$\approx -\frac{1}{\alpha}\cdot\frac{1}{2w_1w_2^*d\cos^2\alpha}\left(\frac{w_1^2+w_2^{*2}}{w_1+w_2^*}\right)\left[\left(2\bar{a}_1-\frac{\boldsymbol{p}}{\cos\alpha}\bar{e}_1\right)y_1+\left(2\bar{a}_2+\frac{\boldsymbol{p}}{\cos\alpha}\bar{e}_2\right)(y_1-y)\right] \tag{32}$$

Setting $\alpha=0$ eliminates the LHS in the above relation, which expectedly degenerates into expression (26). However, with increasing values of α ($>>1/d$) the LHS starts to dominate the RHS, and eventually (32) is reduced to the following approximate yet accurate relation between the transverse displacement of the two tilted-beam modules.

$$\frac{y_1}{w_1}+\frac{y_1-y}{w_2^*}\approx 0$$

Thus, the purely kinematic dependence of θ on y resulting from the tilted-beam configuration suppresses the redistribution of the overall transverse displacement between the two modules due to elastokinematic effects in the presence of an axial load, as seen in the double parallelogram flexure. This has been made possible due to the coupling between the end-moments and transverse displacements revealed in expressions (31). The transverse displacements, thus determined, are then used in estimating the axial direction force-displacement relationships and constraint behavior.

$$x_1 \approx -\frac{\boldsymbol{p}}{2d\cos^2\alpha} + \frac{y_1^{\,2}}{\cos^3\alpha}\left[\left(i - 2k\frac{\alpha}{w_1} + j\frac{\alpha^2}{w_1^2}\right) - \frac{\boldsymbol{p}}{2\cos\alpha}\left(r - 2q\frac{\alpha}{w_1} + s\frac{\alpha^2}{w_1^2}\right)\right]$$

$$x + x_1 \approx \frac{\boldsymbol{p}}{2d\cos^2\alpha} + \frac{(y_1 - y)^2}{\cos^3\alpha}\left[\left(i + 2k\frac{\alpha}{w_2^*} + j\frac{\alpha^2}{w_2^{*2}}\right) + \frac{\boldsymbol{p}}{2\cos\alpha}\left(r + 2q\frac{\alpha}{w_2^*} + s\frac{\alpha^2}{w_2^{*2}}\right)\right] \tag{33}$$

$$\Rightarrow x \approx \frac{\boldsymbol{p}}{d\cos^2\alpha} + \frac{1}{\cos^3\alpha}\left[\left\{-\bar{i}_1 y_1^{\,2} + \bar{i}_2 (y_1 - y)^2\right\} + \frac{\boldsymbol{p}}{2\cos\alpha}\left\{\bar{r}_1 y_1^{\,2} + \bar{r}_2 (y_1 - y)^2\right\}\right]$$

In the above expressions, $\bar{a}_1$, $\bar{c}_1$, $\bar{e}_1$, $\bar{h}_1$, $\bar{i}_1$ and $\bar{r}_1$, are as defined in (24) with $w = w_1$ and beam tilt-angle α, while $\bar{a}_2$, $\bar{c}_2$, $\bar{e}_2$, $\bar{h}_2$, $\bar{i}_2$ and $\bar{r}_2$ are defined with $w = w_2^*$ and a beam tilt-angle of $-\alpha$.

For uniform thickness beams with a typical geometry of $t=1/50$, $w_1=0.5$, $w^*_2=0.28$, and a range of α, the axial stiffness predicted by expression (33) is plotted in Fig. 23. It is seen that with increasing beam tilt-angle α, there is a remarkable improvement in the quality of x DOC in terms of stiffness, especially in comparison to a double parallelogram flexure module. It is also interesting to note that this flexure configuration does not entirely cancel the purely kinematic component of the axial displacement. Thus, an improvement in the stiffness along a DOC is achieved at the expense of larger parasitic error motion. Nevertheless, this flexure module presents a good compromise between the desirable performance measures.

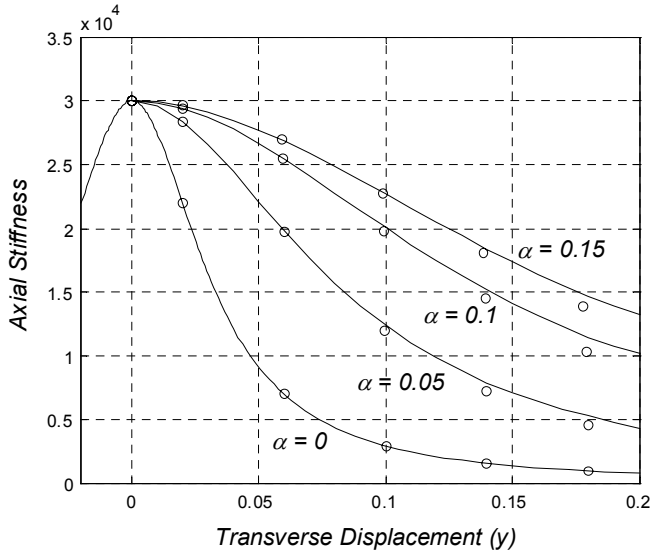

Fig.23 Double Tilted-beam Flexure Axial Stiffness: CFA (Lines), FEA (Circles)

The mathematical results presented above are amply supported by physical arguments. For a given y displacement, when a rotation constraint is imposed on the primary stage, the secondary

stage has a virtual center of rotation located approximately at point C_1, owing to module 1, and a different virtual center of rotation located approximately at point C_2 due to module 2. Since, these two centers of rotation for the rigid secondary stage are spaced apart, the secondary stage is better constrained. Consequently, the additional elastokinematic term encountered in the double parallelogram flexure is attenuated because the dependence of the transverse displacements on the axial load $\boldsymbol{p}$ is reduced. In the limiting case of α approaching zero, points C_1 and C_2 move out to infinity, and no longer pose conflicting constraints on the secondary stage, which therefore becomes free to translate in the transverse direction. This is the case of the double parallelogram flexure, for which it is not possible to constrain the secondary stage by imposing displacements or moments on the primary stage because the transverse displacement and rotation of the constituent parallelograms are not kinematically related and moments do not significantly affect translation.

Of course, the effectiveness of the above strategy for improving the axial stiffness depends upon the rotational constraint on the primary stage of the double tilted-beam flexure. Any mechanism that utilizes this module should be carefully designed to meet this requirement. Mirroring the design about the Y-axis, in Fig. 22, offers limited success because the resulting configuration does not entirely constrain the primary stage rotation. A hybrid design comprising of a double parallelogram flexure and a double-tilt beam flexure may work better because the former can provide the rotation constraint necessary for the latter to preserve the axial stiffness. Of course, this comes with a loss of symmetry, which influences the axial parasitic error motion, thermal and manufacturing sensitivity, among other performance measures. Once again, this discussion highlights the performance tradeoffs in flexure mechanism design.

6. Conclusion

We have presented a non-dimensional analytical framework to predict the performance characteristics of beam-based flexure modules and mechanisms. It has been shown that the load-stiffening and elastokinematic effects, which are not captured in a traditional linear analysis, strongly influence the force-displacement relations, and therefore the constraint properties, of the beam flexure. These non-linear effects are modeled in a simple yet accurate format using mathematical approximations for transcendental functions. The proposed formulation quantifies key metrics including dimensionless elastic stiffness, geometric stiffness, kinematic and elastokinematic coefficients, and relates them to the performance characteristics of the beam flexure. Significantly, it is shown using a specific beam-shape generalization that only these characteristic dimensionless coefficients vary with changing beam shapes, without affecting the nature of the force-displacement relations. This provides a continuous comparison between a lumped-compliance and increasingly distributed-compliance flexure topologies, and an accurate analytical means for modeling elastic averaging. Furthermore, these coefficients provide the objective functions for beam shape optimization using standard techniques.

The results for a generalized beam are employed to analyze several important beam-based flexure modules such as the parallelogram and double parallelogram flexures and their respective variations. The closed-form parametric results provide a qualitative and quantitative understanding of the modules' force-displacement relations and constraint properties. The effects of geometric variations, reversal and symmetry are also mathematically addressed. This provides a basis for a geometric sensitivity analysis to predict the consequences of manufacturing and assembly tolerances, and offers a systematic means for introducing predetermined geometric imperfections in a flexure design to achieve specific desired attributes such as lower error motions or improved DOC stiffness.

An important theme that is repeatedly highlighted in this paper is the existence of performance tradeoffs in flexure design. Performance characteristics of beam-based flexure modules have been characterized and it is shown by means of illustrative examples that the quality requirements for DOF and DOC, in terms of range of motion, error motions and stiffness, are often contradictory. An attempt to improve one performance characteristic inevitably undermines

the others. However, a design that offers a suitable compromise for a given application may be objectively achieved using the analytical results presented in this paper.

Based on an estimate of modeling errors at each step in the analysis, the closed-form predictions presented here are expected to be accurate within *5-10%*, depending on the flexure module. This is corroborated by a thorough non-linear Finite Element Analysis performed in ANSYS using BEAM4 elements, with the large displacement analysis option turn on and shear coefficients set to zero. Although shear effects, which become increasingly important in short beams, have not been included, these can be readily incorporated within the presented framework. While the proposed analysis does not match the generality of computational methods, it allows quick calculations and parametric insights into flexure mechanism behavior, and therefore is potentially helpful in flexure design.

The non-linear load-stiffening and elastokinematic effects may be used to accurately model the dynamic characteristics of flexure mechanisms, which are often employed in precision motion control and vibration isolation. Furthermore, the thermal sensitivity of flexure modules may also be modeled by including the material thermal behavior. Beam shape generalizations and module geometry variations beyond what are presented here may be investigated. A systematic treatment of the concepts of mobility, overconstraint and elastic averaging in flexure mechanisms is currently being developed.

Appendix

This appendix provides a comparison between the Taylor Series expansions of the actual transcendental functions and their algebraic approximations for the compliance, stiffness and constraint terms discussed in Section 2. As mentioned earlier, normalized axial force $\boldsymbol{p} \triangleq k^2$.

c_{11}	Exact	$\left(\frac{k-\tanh k}{k^3}\right)=\frac{1}{3}-\frac{2}{15}\boldsymbol{p}+\frac{17}{315}\boldsymbol{p}^2-\frac{62}{2835}\boldsymbol{p}^3+\cdots$
	Approximate	$\frac{1}{3\left(1+\frac{2}{5}p\right)}=\frac{1}{3}-\frac{2}{15}\boldsymbol{p}+\frac{4}{75}\boldsymbol{p}^2-\frac{8}{375}\boldsymbol{p}^3+\cdots$
c_{12}	Exact	$\left(\frac{\cosh k-1}{k^2\cosh k}\right)=\frac{1}{2}-\frac{5}{24}\boldsymbol{p}+\frac{61}{720}\boldsymbol{p}^2-\frac{277}{8064}\boldsymbol{p}^3\cdots$
	Approximate	$\frac{1}{2\left(1+\frac{5}{12}\boldsymbol{p}\right)}=\frac{1}{2}-\frac{2}{24}\boldsymbol{p}+\frac{25}{288}\boldsymbol{p}^2-\frac{125}{3456}\boldsymbol{p}^3+\cdots$
c_{22}	Exact	$\left(\frac{\tanh k}{k}\right)=1-\frac{1}{3}\boldsymbol{p}^2+\frac{2}{15}\boldsymbol{p}^2-\frac{17}{315}\boldsymbol{p}^3+\cdots$
	Approximate	$\frac{\left(1+\frac{1}{10}\boldsymbol{p}\right)}{\left(1+\frac{13}{30}\boldsymbol{p}+\frac{1}{96}\boldsymbol{p}^2\right)}=1-\frac{1}{3}\boldsymbol{p}^2+\frac{193}{1440}\boldsymbol{p}^2-\frac{2359}{43200}\boldsymbol{p}^3+\cdots$
k_{11}	Exact	$\frac{k^3\sinh k}{k\sinh k-2\cosh k+2}=12+\frac{6}{5}\boldsymbol{p}-\frac{1}{700}\boldsymbol{p}^2+\frac{1}{63000}\boldsymbol{p}^3$
	Approximate	$12+\frac{6}{5}\boldsymbol{p}$
k_{12}	Exact	$\frac{k^2(1-\cosh k)}{k\sinh k-2\cosh k+2}=-6-\frac{1}{10}\boldsymbol{p}+\frac{1}{1400}\boldsymbol{p}^2-\frac{1}{126000}\boldsymbol{p}^3$
	Approximate	$-6-\frac{1}{10}\boldsymbol{p}$
k_{22}	Exact	$\frac{k^2\cosh k-k\sinh k}{k\sinh k-2\cosh k+2}=4+\frac{2}{15}\boldsymbol{p}-\frac{11}{6300}\boldsymbol{p}^2+\frac{1}{27000}\boldsymbol{p}^3$
	Approximate	$4+\frac{2}{15}\boldsymbol{p}$
r_{11}	Exact	$\frac{k^2(\cosh^2 k+\cosh k-2)-3k\sinh k(\cosh k-1)}{2\left(k\sinh k-2\cosh k+2\right)^2}$ $=\frac{3}{5}-\frac{1}{700}\boldsymbol{p}+\frac{1}{42000}\boldsymbol{p}^2-\frac{37}{97020000}\boldsymbol{p}^3+\cdots$
	Approximate	$\frac{3}{5}-\frac{1}{700}\boldsymbol{p}$

r_{12}	Exact	$-\dfrac{k^2(\cosh k-1)+k\ \sinh k\ (\cosh k-1)-4(\cosh k-1)^2}{4\left(k\sinh k-2\cosh k+2\right)^2}$ $=-\dfrac{1}{20}+\dfrac{1}{1400}\boldsymbol{p}-\dfrac{1}{84000}\boldsymbol{p}^2+\dfrac{37}{194040000}\boldsymbol{p}^3+\ \cdots$
	Approximate	$-\dfrac{1}{20}+\dfrac{1}{1400}\boldsymbol{p}$
r_{22}	Exact	$\dfrac{-k^3+k^2\sinh k(\cosh k+2)-2k\ (2\cosh^2 k-\cosh k-1)}{4k\left(k\sinh k-2\cosh k+2\right)^2}$ $+\ \dfrac{2\sinh k\ (\cosh k-1)}{4k\left(k\sinh k-2\cosh k+2\right)^2}$ $=\dfrac{1}{15}-\dfrac{11}{6300}\boldsymbol{p}+\dfrac{1}{18000}\boldsymbol{p}^2-\dfrac{509}{291060000}\boldsymbol{p}^3+\ \cdots$
	Approximate	$\dfrac{1}{15}-\dfrac{11}{6300}\boldsymbol{p}$

References

1. Slocum, A.H., 1992, *Precision Machine Design*, Society of Manufacturing Engineers, Dearborn, MI.
2. Blanding, D.K., 1999, *Exact Constraint: Machine Design Using Kinematic Principles*, ASME Press, New York, NY.
3. Smith, S.T., 2000, *Flexures: Elements of Elastic Mechanisms*, Gordon and Breach Science Publishers, New York, NY.
4. Ejik, J.V., 1985, "On the Design of Plate Spring Mechanism", Ph.D. thesis, Delft University of Technology, Delft, The Netherlands.
5. Awtar, S., 2004, "Analysis and Synthesis of Planer Kinematic XY Mechanisms", Sc.D. thesis, Massachusetts Institute of Technology, Cambridge MA. (http://web.mit.edu/shorya/www)
6. Bisshopp, K.E., and Drucker, D.C., 1945, "Large Deflection of Cantilever Beams", Quarterly of Applied Mathematics, **3**(3), pp. 272-275.
7. Frisch-Fay, R., 1963, *Flexible Bars*, Butterworth, Washington DC.
8. Mattiasson, K., 1981, "Numerical Results from Large Deflection Beam and Frame Problems Analyzed by Means of Elliptic Integrals", International Journal for Numerical Methods in Engineering, **17**, pp. 145-153.
9. Howell, L.L, 2001, *Compliant Mechanisms*, John Wiley & Sons, New York, NY.
10. Plainevaux, J.E., 1956, "Etude des deformations d'une lame de suspension elastique", Nuovo Cimento, **4**, pp. 922-928.
11. Legtenberg, R., Groeneveld, A.W. and Elwenspoek, M., 1996, "Comb-drive Actuators for Large Displacements", Journal of Micromechanics and Microengineering, **6**, pp. 320-329.
12. Haringx, J.A., "The Cross-Spring Pivot as a Constructional Element", Applied Science Research, **A1**(4), pp. 313-332.

13. Zelenika, S., and DeBona, F., 2002, “Analytical and Experimental Characterization of High Precision Flexural Pivots subjected to Lateral Loads”, Precision Engineering, **26**, pp. 381-388.

14. Jones, R.V., 1988, *Instruments and Experiences: Papers on Measurement and Instrument Design*, John Wiley & Sons, New York, NY.

15. Zhou, G. and Dowd, P., 2003, “Tilted Folded-Beam Suspension for Extending the Stage Travel Range of Comb-drive Actuators”, Journal of Micromechanics and Microengineering, **13**, pp. 178-183.

16. Saggere, L., Kota, S., 1994, “A New Design for Suspension of Linear Microactuators”, ASME Journal of Dynamic Systems and Control, **55**(2), pp. 671-675.

List of Figure and Table Captions

Fig.1 a)Lumped-Compliance and b)Distributed-Compliance Multi-Parallelogram Mechanisms

Fig.2 Generalized Beam Flexure

Fig.3 Normalized Compliance Terms: Actual (Solid Lines) and Approximate (Dashed Lines)

Fig.4 Transverse Elastic Stiffness Coefficients

Fig.5 Transverse Geometric Stiffness Coefficients

Fig.6 Axial Kinematic Coefficients

Fig.7 Axial Elastokinematic Coefficients

Fig.8 Axial Elastic Stiffness Coefficient

Fig.9 Parallelogram Flexure and Free Body Diagram

Fig.10 Parallelogram Flexure Stage Rotation: CFA (Lines), FEA (Circles)

Fig.11 Parallelogram Flexure Transverse Displacement: CFA (Lines), FEA (Circles)

Fig.12 Parallelogram and Double Parallelogram Flexures Transverse Stiffness: CFA (Lines), FEA (Circles)

Fig.13 Parallelogram and Double Parallelogram Flexures Axial Stiffness: CFA (Lines), FEA (Circles)

Fig.14 'Non-identical Beam' Parallelogram Flexure Stage Rotation: CFA (Lines), FEA (Circles)

Fig.15 Tilted-beam Flexure

Fig.16 Tilted-beam Flexure Transverse Elastic Stiffness: CFA (Lines), FEA (Circles)

Fig.17 Tilted-beam Flexure Stage Rotation: CFA (Lines), FEA (Circles)

Fig.18 Tilted-beam Flexure Kinematic Axial Displacement: CFA (Lines), FEA (Circles)

Fig.19 Tilted-beam Flexure Axial Stiffness: CFA (Lines), FEA (Circles)

Fig.20 Double Parallelogram Flexure

Fig.21 Double Parallelogram Flexure Primary Stage Rotation: CFA (Lines), FEA (Circles)

Fig.22 Double Tilted-beam Flexure

Fig.23 Double Tilted-beam Flexure Axial Stiffness: CFA (Lines), FEA (Circles)

Table 1. Stiffness, Kinematic and Elastokinematic Coefficients for a Simple Beam